NPL Report CMMT(A)275

REPORT

# The Prediction of the Thermophysical Properties and the Solidification of Commercial Alloys

P N Quested, A T Dinsdale, J A J Robinson

K C Mills*, J D Hunt**

*Department of Metallurgy and Materials Science, Imperial College of Science and Technology

** Department of Materials, University of Oxford

July 2000

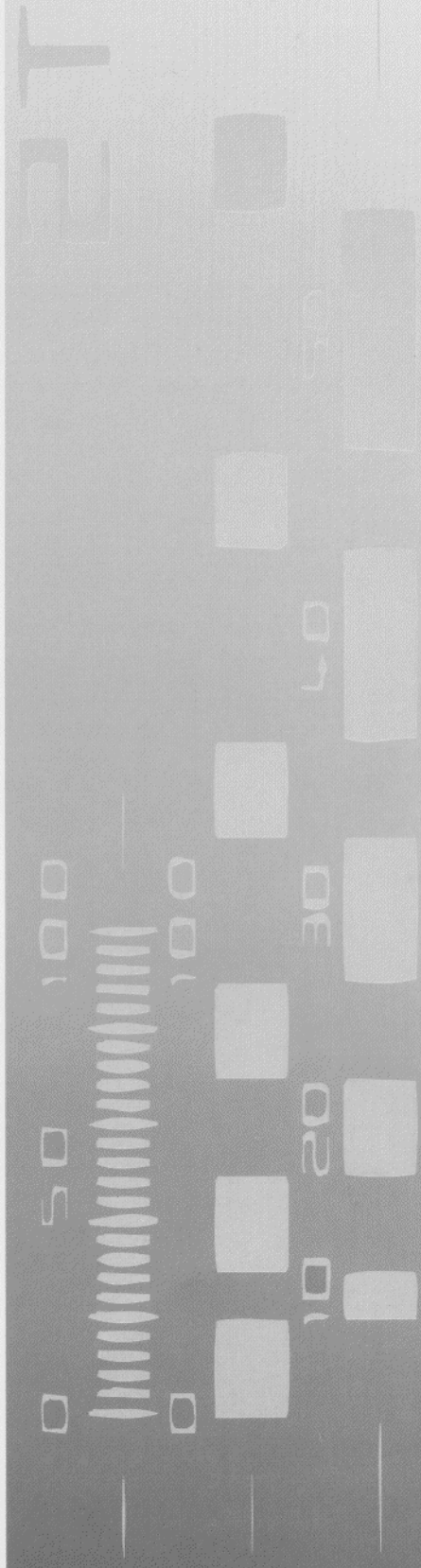

NPL
National Physical Laboratory

CMMT(A)275
July 2000

# THE PREDICTION OF THE THERMOPHYSICAL PROPERTIES AND THE SOLIDIFICATION PATH OF COMMERCIAL ALLOYS

P N Quested, A T Dinsdale, J A J Robinson
Centre for Materials Measurement and Technology,
National Physical Laboratory, Teddington, Middlesex

K C Mills
Department of Metallurgy and Materials Science
Imperial College of Science and Technology
Prince Consort Road, London SW7 2BP

and

J D Hunt
Department of Materials,
University of Oxford, Oxford OX1 3PH

## ABSTRACT

The behaviour of the multicomponent alloys used by industry can often be quite complex. For example during solidification the chemical composition of the liquid phase may vary considerably. A knowledge of the way in which variations of composition affect thermophysical properties can help industry to avoid any harmful side effects and may also act as a valuable aid to process optimisation. It is, however, expensive to provide all the required data by direct measurement, especially in cases where the industrial liquid is highly corrosive or dangerous to handle in a laboratory environment.

A number of models have been developed to estimate the enthalpies, heat capacities, densities, viscosities, thermal and electrical conductivities of multicomponent, commercial alloys in the solid and liquid states. Many of these have been reviewed here and some of the estimated values compared with measured values for the properties of various commercial alloys.

The report also includes, as an appendix, a review of experimental and numerical methods for determining the solidification path in commercial alloys provided by Dr J D Hunt.

The report is intended to be used in conjunction with Virtual Measurement System software developed at NPL to provide key information to engineers and metallurgists concerned with the solidification of commercial alloys. The tools, based on the models described in this report combined with critically assessed data developed and compiled at NPL over the years, are being validated simultaneously via a programme of measurement on specific materials chosen such that they are representative of those used by industry.

NPL Report CMMT(A)275



ISSN 1361-4061

Centre for Materials Measurement and Technology
National Physical Laboratory
Teddington
Middlesex TW11 0LW



Approved on behalf of the Managing Director, NPL,
by Dr C Lea, Head, Centre for Materials Measurement and Technology

# 1 INTRODUCTION

Over the last two decades mathematical modelling has become an established tool for improving both process control and product quality. These models have been applied to a wide variety of processes and industries such as the casting and foundry production, steelmaking, secondary refining of non-ferrous metals, welding, spray forming dip coating, metallic powder and ribbon production. Model development has evolved to the point where one of the prime requirements at the present time is for accurate physical property data for the commercial alloys involved in these processes. Data are required for the factors affecting the fluid flow and heat transfer in the process ie density, viscosity, surface tension, enthalpy, heat capacity, thermal conductivity, thermal diffusivity. The absence of reliable data for commercial alloys reflects the difficulties encountered in obtaining accurate values for these properties at high temperatures; for instance Vida and Guthrie [89iid/gut] have shown that the reported viscosities of pure iron and aluminium vary by ±50% and ±l00% around the mean. Even greater uncertainties would be expected with commercial alloys which are subject to segregation, and the presence of non-metallic inclusions etc.. The Department of Trade and Industry has recognised this need for accurate thermophysical property data for commercial materials and has funded research programmes to develop methods necessary to provide this information [95que/mil].

Industry frequently needs to react quickly to combat specific problems in process control or product quality. Even when experimental methods are available the production of accurate data is frequently time-consuming. Consequently, there is a need for the development of mathematical models to predict the thermophysical properties of alloys from their chemical composition and melting range, since frequently this is the only information available. However, accurate values may only be estimated if the data used in the model is based on reliable, traceable values for the material. Consequently a three-pronged approach has been adopted:

(i) accurate measurement of thermophysical properties

(ii) critical evaluation of literature data and

(iii) the development of estimation routines based on accurate property data from (i) and (ii)

Since many process models involve the solidification of liquid metals, it is necessary to estimate values for the solid, liquid and 'mushy' phases. It would also be advantageous if such a model had universal application ie it could be applied to a wide range of alloys spanning from aluminium alloys to steels.

This report describes the various models which have been developed to estimate heat capacities, enthalpies, densities, viscosities, surface tension and thermal and electrical conductivities.

In order to obtain accurate estimated values it is necessary to use accurate information for the thermophysical properties of alloys in the development of the model. Consequently, property values obtained in the parallel measurement programme have been used for the purpose [95que/mil, 95que].

## 2 GENERAL DESCRIPTION OF MODELS

Most methods for estimating thermophysical properties use as a starting point well defined standard reference data for the pure elements.

The following reference sources in Table 1 have also been used in this development of models.

Table 1

Data sources used in model development

| Property | Pure elements | Commercial alloys |
|---|---|---|
| Heat capacity, enthalpy | [93kub / alc] [91din] | [95que] |
| Density | [80tur] [89iid / gut] | [95que] [74stu] |
| Viscosity | [89iid / gut] [88kaw / shi] | [95que] |
| Thermal and electrical conductivity | [89iid / gut] [34mot] [96mil / kee] | [70tou / pow], [60pow], [88bog / ho], [93bog / des], [87fil / roc] [89fil / roc], [71lud / sch] |

Such data for the elements will differ from one phase to another and will also vary as a function of temperature. Therefore, for example, the molar volume of pure Fe will differ according to whether the phase in question is the bcc phase (ferrite), the fcc phase (austenite) or liquid.

The variation of a particular property with temperature is often different from one property to another although it will often involve some power series expression to allow interpolation and extrapolation.

The general form of the composition dependence can be expressed as:

$$\Omega^p = \Omega_1^p x_1 + \Omega_2^p x_2 + \Omega_3^p x_3 + \ldots\ldots\ldots + \Omega_{ideal}^p + \Omega_{excess}^p \qquad (1)$$

where $\Omega^p$ represents the property $\Omega$ of phase p for the composition ($x_1$, $x_2$, $x_3$, ….) usually expressed in terms of mole fraction. The property $\Omega_i^p$ is the value of the property for the pure element i. For a number of properties eg heat capacity, this may be sufficient to provide an acceptable estimate of the property in the multicomponent system especially if the experimental data are sparse or of limited accuracy. For other properties where experimental data are available it may be appropriate to add a corrected term to compensate for the effect of any interaction between the elements on the property. This may contain a theoretical component eg for the molar Gibbs energy.

This approach requires that data are available for each property for each element for all the phases in which a given element can dissolve. Furthermore these data must be available for a wide range of temperatures. In the case of iron, for example, it is necessary that volumetric data are available for the austenite, ferrite and liquid phases even for temperatures where the phase in question is not stable for pure Fe. An example of this is

where data for fcc Fe is required at relatively low temperatures to model the variation of molar volume data of aluminium alloys.

A more complicated example of this occurs where data would be required for an element in a phase in which it is never stable. For example, silicon will dissolve to a limited degree in aluminium. To model the molar volume of aluminium-silicon fcc alloys it is necessary to use data for fcc silicon even though pure silicon never forms in that structure. Often it is possible to assume that the data for one phase of an element is identical to that for the stable phase eg it may be a reasonable assumption that the molar volume of fcc silicon is the same as that for the stable diamond structure. For other properties eg enthalpy this assumption could be quite wrong. The derivation of data for unstable and metastable phases of elements has been studied in great detail for thermodynamic properties and good standard reference data are available (91din).

## 3 ESTIMATION OF HEAT, CAPACITIES, ENTHALPIES

The temperature dependence of heat capacities of most elements can usually be satisfactorily expressed in the form shown in Equation 2 where a, b, c and d are constants, T is the temperature in kelvins.

$$C_p = a + bT + cT^2 + \frac{d}{T^2} \qquad (2)$$

Often it is convenient to use a number of such expressions for a particular element each valid over a particular temperature range.

Values a, b, c and d for a multicomponent alloy can be obtained from Equations 3-6

$$a = a_1x_1 + a_2x_2 + a_3x_3 \qquad (3)$$
$$b = b_1x_1 + b_2x_2 + b_3x_3 \qquad (4)$$
$$c = c_1x_1 + c_2x_2 + c_3x_3 \qquad (5)$$
$$d = d_1x_1 + d_2x_2 + d_3x_3 \qquad (6)$$

The enthalpy ($H_T$-$H_{298}$) can be calculated using Equation 7

$$H_T - H_{298} = \int_{298}^{T} C_p dT = a(T-298) + \frac{b}{2}(T^2 - 298^2) + \frac{c}{3}(T^3 - 298^3) - d\left(\frac{1}{T} - \frac{1}{298}\right) \qquad (7)$$

For certain elements which have appreciable contributions arising from magnetic interactions eg Fe, Ni, Co it is generally more accurate to apply equations (3) to (7) to the hypothetical paramagnetic form and to apply a separate magnetic contribution to the thermodynamic properties depending on whether the phase at the composition and temperature of interest is paramagnetic, ferromagnetic or antiferromagnetic.

As a first approximation the enthalpy of fusion ($\Delta H_{fus}$) may be estimated from the entropy of fusion ($\Delta S_{fus}$) as shown in Equations 8 and 9 where $T_{liq}$ is the liquidus temperature

$$\Delta S^{fus} = x_1\Delta\bar{S}_1^{fus} + x_2\Delta\bar{S}_2^{fus} + x_3\Delta\bar{S}_3^{fus} + \ldots\ldots \qquad (8)$$

$$\Delta H^{fus} = T_{liq}\Delta S^{fus} \qquad (9)$$

Using this approximation, values for the enthalpy of liquid alloys may be calculated from Equation 10 where sol and l denote the solid and liquid phases, respectively.

$$(H_T - H_{298}) = Cp^{sol}_{alloy}(T_{liq} - 298) + T_{liq}\Delta S^{fus}_{alloy} + Cp^{l}_{alloy}(T - T_{liq}) \qquad (10)$$

However this approach will not work well for alloys where there are appreciable enthalpies of mixing in the liquids or solid phases. Also this method will not provide information about the variation of liquidus and solidus temperature with composition or details of the enthalpy release as a function of temperature. For these cases a more rigorous thermochemical phase equilibrium approach is to be preferred.

It has been found that the predicted values of Cp and ($H_T$-$H_{298}$) are typically within 2% of measured values for a wide variety of alloys. However, the model predicts neither the occurrence of phase transitions nor the enthalpies associated with these transitions. It can be seen from Figure 1 that predicted values are in excellent agreement with measured values. Overall enthalpy ($H_T$-$H_{298}$) values for liquid aluminium bronze were also in excellent agreement with measured values.

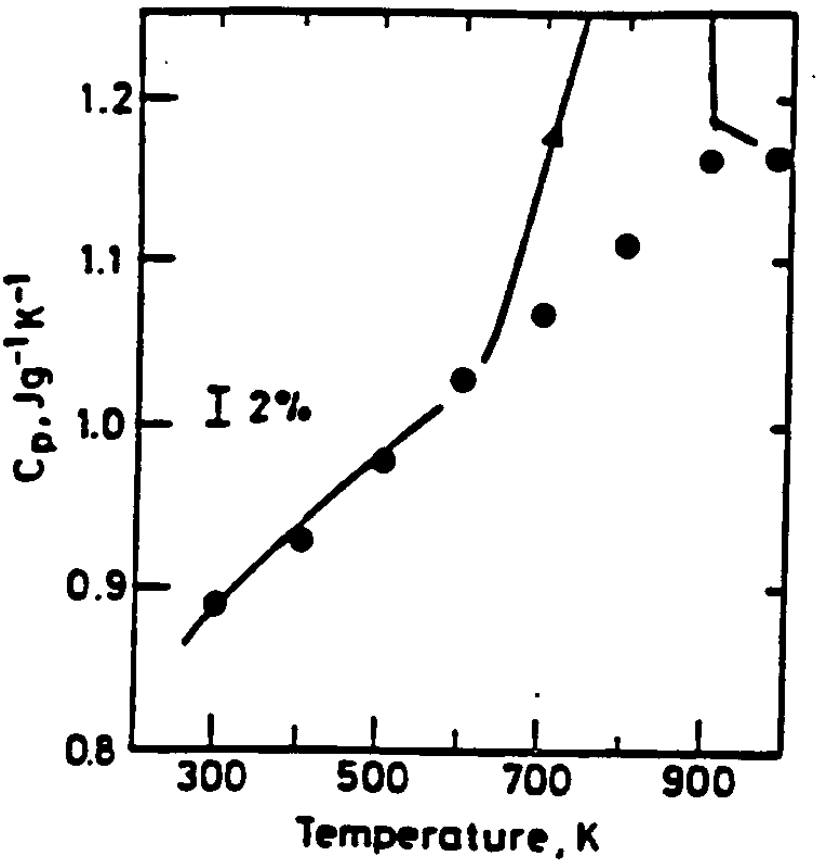


Figure 1 Heat capacity of Al + Si alloy as function of temperature; The symbols indicate measured values, the solid curve indicates estimated values.

## 4 PHASE EQUILIBRIUM APPROACH

During a solidification process a number of different phases may be present at any one time eg the liquid and one or more crystalline phases. The simplest approach to model the process is to assume that the system is in chemical equilibrium which can be computed provided the required thermodynamic data are available. Under certain conditions it may be more appropriate to consider other models for the solidification to allow for the different rates of chemical diffusion between the various elements in the different phases (cf the appendix).

For a pure element solidification takes place at a single temperature and the enthalpy of fusion ie the amount of heat necessary to melt the material, is simply the difference in enthalpy between the liquid and crystalline phases at that temperature. In general for an alloy with more that one element solidification will occur over a range of temperatures ie between the liquidus temperature when the first solid appear to the solidus temperature when the last liquid disappears. The enthalpy of fusion for such an alloy could, in principle, be viewed in two different ways

a) as the amount of heat required to transform a solid sample at the solidus temperature to a liquid state at the liquidus temperature ie the amount of heat required to melt a material or
b) as the difference in enthalpy between the pure liquid phase and the mixture of solid phases at a single temperature ie an isothermal enthalpy of fusion. The choice of this temperature is, to some, extent, arbitrary but could for example, be the liquidus temperature, the solidus temperature or some temperature between the solidus and liquidus temperatures where the appropriate enthalpy curves are extrapolated as necessary. This is illustrated in Figure 2. The enthalpy of fusion will differ slightly according to the chosen temperature ie there is no definitive value for the enthalpy of fusion for a material which melts over a range of temperatures.

As indicated in Figure 2 the details of the enthalpy release with temperature during solidification is complicated and this is even more evident in figure 3 which shows the calculated heat capacity (ie the gradient of the enthalpy curve) over that same temperature range. This heat capacity is made up firstly from the contributions arising from the pure phases themselves ie the heat capacity in the level sections either side of the freezing range and secondly as a result of the heat absorbed or given out associated with the gradual change from the solid state to the liquid state.

Some of the thermophysical properties of the system in this case can be calculated as simply the sum of the properties of the individual phases eg volume while other properties may depend on the detailed microstructure of the material eg thermal conductivity. Other properties eg viscosity and surface tension are really appropriate only to the liquid phase.

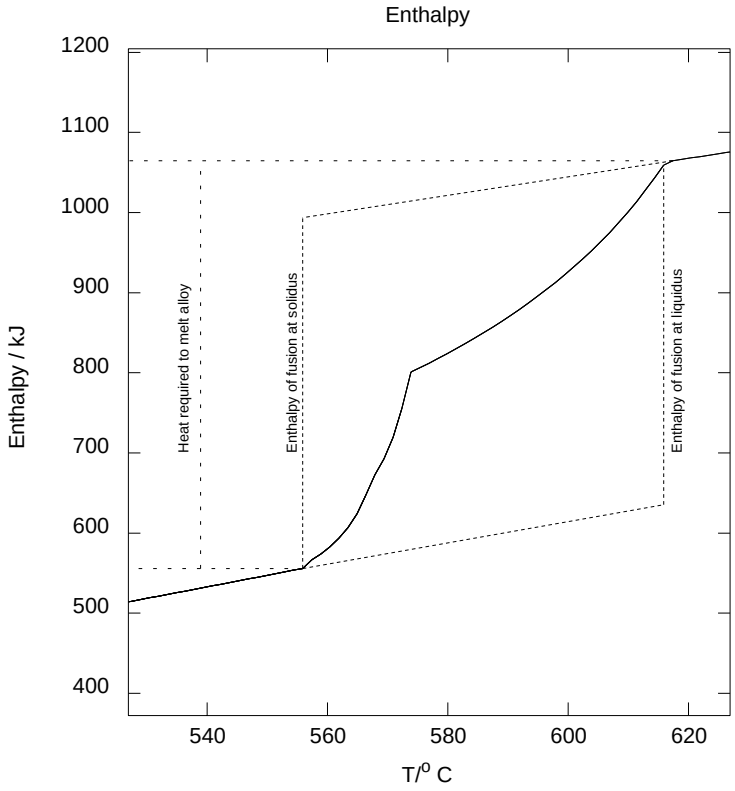


Figure 2 Calculated enthalpy curve associated with the fusion of a multicomponent alloy

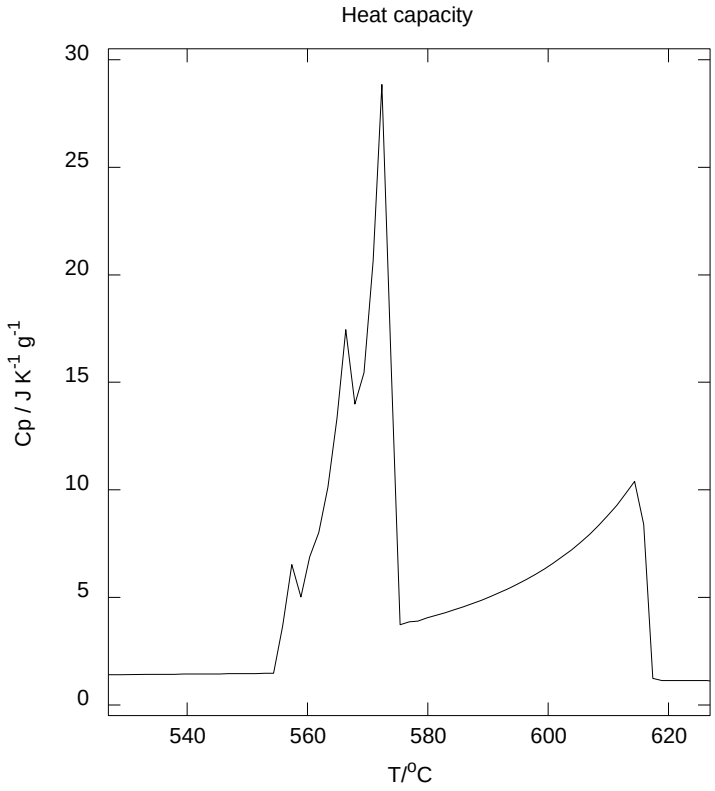


Figure 3 Calculated heat capacity during the fusion of a multicomponent alloy

## 4 ESTIMATION OF DENSITIES

Various models have been used to calculate molar volumes (V) and densities (ρ) for liquid and solid alloys. One approach is to use Equations 11-14 where M is the molecular weight (= $x_1M_1 + x_2M_2 + x_3M_3 + ...$) and β is the volume expansion coefficient ($\beta = x_1\beta_1 + x_2\beta_2 + x_3\beta_3$). β itself may be expressed as a function of T is greater accuracy is required.

$$V = x_i V_1 + x_2 V_2 + x_3 V_3 \quad (11)$$

$$\rho = (M / V) \quad (12)$$

solid: $$V = V_{298}(1 + \beta_{sol}(T - 298)) \quad (13)$$

liquid: $$V = V_{liq}^{T}(1 + \beta_l(T - T_{liq})) \quad (14)$$

The prediction of the model expressed in equations (10-13) have been compared with experimental density data for the solid and liquid phases. The estimated densities for solid alloys always lay within 5% of the measured values. Estimated density (ρ) values for nickel-based alloys at 298 K tended to be lower than measured values and this was attributed to the fact that Al took up interstitial positions in the lattice. This view was corroborated by the fact that ($\rho_{meas}$-$\rho_{calc}$) was found to increase with increasing Al content; using Equation 15 it should be possible to estimate densities of solid superalloys to ±1-2%.

$$\rho_{meas} = (1 + 0.0116\%\mathrm{Al})\rho_{calc} \quad (15)$$

It has proved difficult to check the validity of the model for the liquid phase densities due to the paucity of experimental data for commercial alloys. Density values for various liquid commercial alloys have been found to lie within 5% of the measured values.

Miettinen [94mie/lou, 97mie], on the other hand, has preferred to express density for a range of carbon and lower alloy steels as a power series expression of the form:

$$\rho = \rho_{Fe} + \sum k_i C_i \quad (16)$$

where $\rho_{Fe}$ is the density of pure Fe, $k_i$ describes the effect of the solute i and $C_i$ is the composition of the solute in weight percent. A similar approach has been used for copper alloys [99har/mie].

Figure 4 demonstrates the success of Miettinen's approach albeit for a limited composition range of steels

A similar approach has been used by Sung and Poirier et al for modelling the densities of liquid [97sun/poi] and solid [98sun/poi] nickel-base superalloys. For liquid superalloys the authors analysed density data for five commercial alloys, initially estimating molar volume data from values for the pure elements, fitting these data to an expression similar to that used by Miettinen and then correcting the predicted densities by applying an equation derived through a regression fit of observed excess volumes of mixing. The authors used a slightly different approach for solid phase alloys preferring to fit the

observed lattice parameter at 20°C as a function of composition together with the experimental coefficients of thermal expansion. This appears to work well for single phase alloys. The density of two phases γ+γ' alloys varies according to the proportion of γ' [75mor/spo].

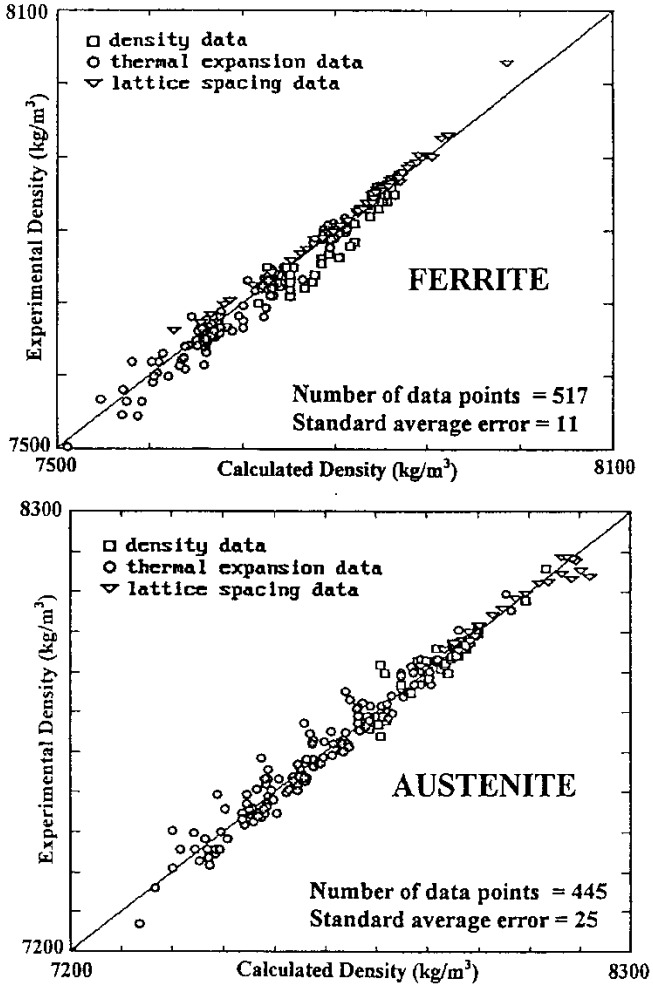


Figure 4 Fit of experimental data for the density of ferritic and austenitic steels by Miettinen

## 5 ESTIMATION OF VISCOSITIES

Andrade [34and] derived the following relationship between the viscosity of a liquid metal at its melting point ($T_{liq}$), the atomic weight (M) and molar volume of the liquid (V):

$$\eta_{Tliq} = \frac{B(MT_{liq})^{0.5}}{V_{Tliq}^{2/3}} \qquad (17)$$

where B is constant determined from experimental viscosity.

From the absolute rate theory proposed by Glasstone et al [41gla/lai]:

$$\eta = A \quad \exp\left(\frac{\Delta G^*}{RT}\right) \tag{18}$$

where $\Delta G^*$ is the Gibbs energy of activation and R is the Gas Constant and A is a constant of proportionality. From the analysis of a number of metals Iida and Guthrie [89iid/gut] obtained

$$\Delta G^* = 5.06264\, T_{liq}^{\ 1.2} \quad \mathbf{J\ mol^{-1}} \tag{19}$$

and

$$\mathbf{A} = \frac{\mathbf{5.7x10^{-6}(MT_{liq})^{0.5}}}{\mathbf{V_{Tliq}^{2/3}\exp\left\{\frac{(1.21T_{liq}^{\ 1.2})}{RT_{liq}}\right\}}} \tag{20}$$

where the volume is expressed in $m^3\ mol^{-1}$ and the viscosity is in mPa s.

This can be used to predict the viscosity of multicomponent alloy if, for a given temperature, contributions to the overall viscosity for each component are calculated using equation 18 and summed together using equation 1.

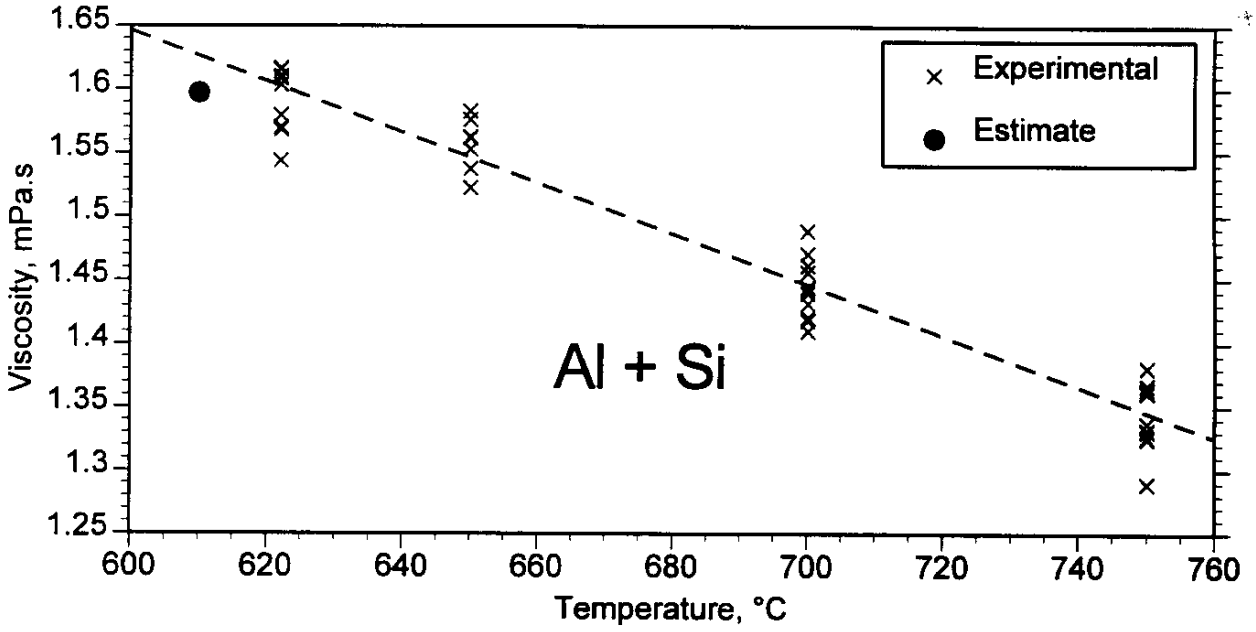


Figure 5 Viscosities of Al+Si alloy as a function of temperature

It is difficult to check the validity of the predicted values since it is not known what are the experimental uncertainties in the viscosity values for (i) the pure elements used in the model testing and (ii) the commercial alloys. (Note the experimental scatter bands around the mean for Fe(liq) and Al(liq) are ±50%, and ±100% respectively.) Nevertheless, it can be

seen from Figure 5 that the estimated viscosities lie within 10% of the measured value for a molten Al +Si alloy [95que]

A related approach has been adopted by Hirai [93hir] who used equation 18 with

$$\Delta G^* = 2.65\, T_{liq}^{\,1.27} \qquad \text{J mol}^{-1}$$

and

$$\mathbf{A} = \frac{\mathbf{1.7x10^{-7}}\,\rho^{\mathbf{2/3}}\mathbf{T_{liq}M^{-1.6}}}{\exp\left\{\dfrac{\mathbf{2.65T_{liq}^{1.27})}}{\mathbf{RT_{liq}}}\right\}} \tag{21}$$

where, in this case, $T_{liq}$ is the liquidus temperature of the alloy. This implies that the viscosity will tend to follow the liquidus surface. Seetharaman [94see/du] has shown that, while it gives good agreement in some cases, it can give completely incorrect composition dependence for systems showing eutectic behaviour eg Bi-Sn.

A rather different approach has been used by Seetharaman and colleagues [94see/du]. For this model A is given by:

$$A = \frac{hN}{V_m} \tag{22}$$

where h is the Planck constant, N the Avogardo number and $V_m$ the molar volume of the alloy at the appropriate temperature.

They further suggested that $\Delta G^*$ is related closely to the Gibbs energy of mixing in the liquid at the appropriate temperature through the equation:

$$\Delta G^* = \sum x_i \Delta G_i^* + \Delta^m G_{mix} + 3RTx_1x_2 \tag{23}$$

where $\Delta G_i^*$ is the Gibbs energy of activation for each of the pure components i and $\Delta^m G_{mix}$ is the Gibbs energy of mixing.

Seetharaman [94see/du] has applied the model to a number of binary alloy systems with good success as shown in Figure 6 and used it to extrapolate in multicomponent systems.

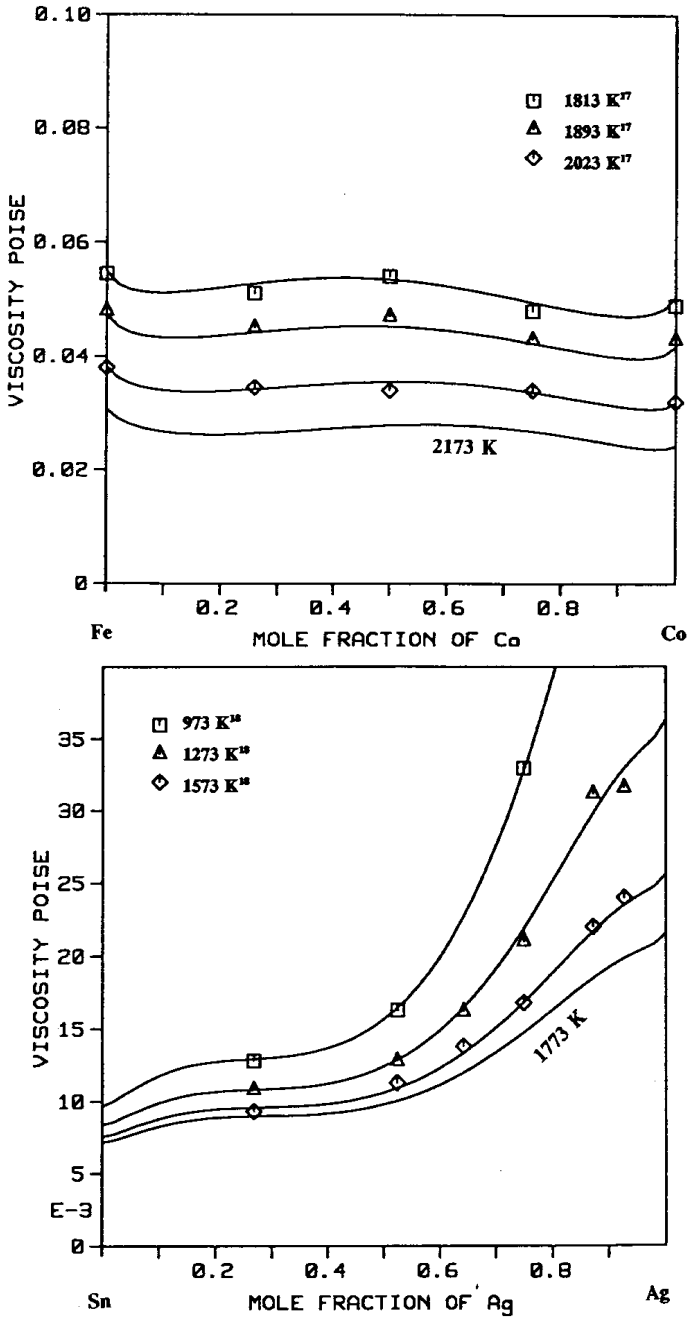


Figure 6. A comparison between calculated and experimental viscosities for the Co-Fe and Ag-Sn systems from Seetharaman et al (94see / du).

## 6 THERMAL AND ELECTRICAL CONDUCTIVITIES

Thermal conductivities of liquid metals are difficult to measure accurately since the measured heat flux frequently contains contributions from convection and these difficulties become increasingly important at the high temperatures. In recent yeas it has been shown that transient techniques provide the most accurate values for liquid alloys since they minimise contributions from convection.

## 6.1 LIQUID ALLOYS

At high temperatures the principal mechanism for thermal conduction in liquid metals is due to the transport of electrons. Although phonon (or lattice) conduction can make a significant contribution at lower temperatures, a recent review [96mil/kee] concluded that electronic conduction is the dominant mechanism for temperatures around the melting point. Consequently, the Wiedemann-Franz-Lorenz (WFL) Rule relating thermal ($\lambda$) and electrical ($\sigma$) conductivities can be used with confidence to predict thermal conductivities of molten alloys. The WFL relation is shown in Equation 24 where $L_0$ is a constant with a theoretical value of 2.445E-8 $W\Omega K^{-2}$ and T is the temperature in kelvins.

$$\lambda = L_0 \, T \, \sigma \tag{24}$$

The electrical conductivities (unlike thermal conductivities) should not be affected by convective flows in the molten metal pool. Consequently, it should be possible to calculate thermal conductivities for molten alloys from the electrical conductivity values. Iida and Guthrie [89iid/gut] have reported electrical conductivity data for molten binary alloys and the values indicate that most alloys exhibit relatively small (< 10%) negative departures from linearity (Equation 25).

$$\sigma_{T_{liq}} = \overline{\sigma_1} x_1 + \overline{\sigma_2} x_2 + \overline{\sigma_3} x_3 ..... \tag{25}$$

The temperature dependence can be calculated using Equation (26).

$$\sigma_T = \sigma_{T_{liq}} \left( 1 + \left( \frac{d\sigma}{dT} \right)_{alloy} \right) \tag{26}$$

where

$$(d\sigma / dT) = x_1 (d\sigma_1 / dt) + x_2 (d\sigma_2 / dT) + x_3 (d\sigma_3 / dT) + .... \tag{27}$$

The thermal conductivity for the liquid is calculated by inserting $\sigma_T$ and the temperature, T into Equation 24. However, it should be noted that this calculation will tend to produce a slightly high value for the thermal conductivity because the electrical conductivities have been observed to exhibit negative departures from linearity as represented by Equation 25.

An alternative method of calculating the thermal conductivity of liquid alloys is to use [34mot] Equation (28) where K is a constant, m denotes the value at melting point and $\Delta S^{fus}$ can be calculated from Equation 8.

$$\ln(\lambda^m_{sol} / \lambda^m_{liq}) = K \Delta S^{fus} \tag{28}$$

Values of K have been derived from $\lambda$ and $\Delta S^{fus}$ values obtained for low melting, metallic element; K had a mean value of 0.073 K mol $J^{-1}$. The only disadvantage with this technique is that it requires a knowledge of the thermal conductivity of the solid ($\lambda^m_{sol}$) at the liquidus temperature.

Estimated thermal conductivity values (via Equation 28) are compared with experimental values obtained for the commercial Al-Si alloy in Figure 7 and it can be seen that they are slightly higher than the experimental values but the value derived from the entropy of fusion (Equation 28) is in good agreement with the experimental values.

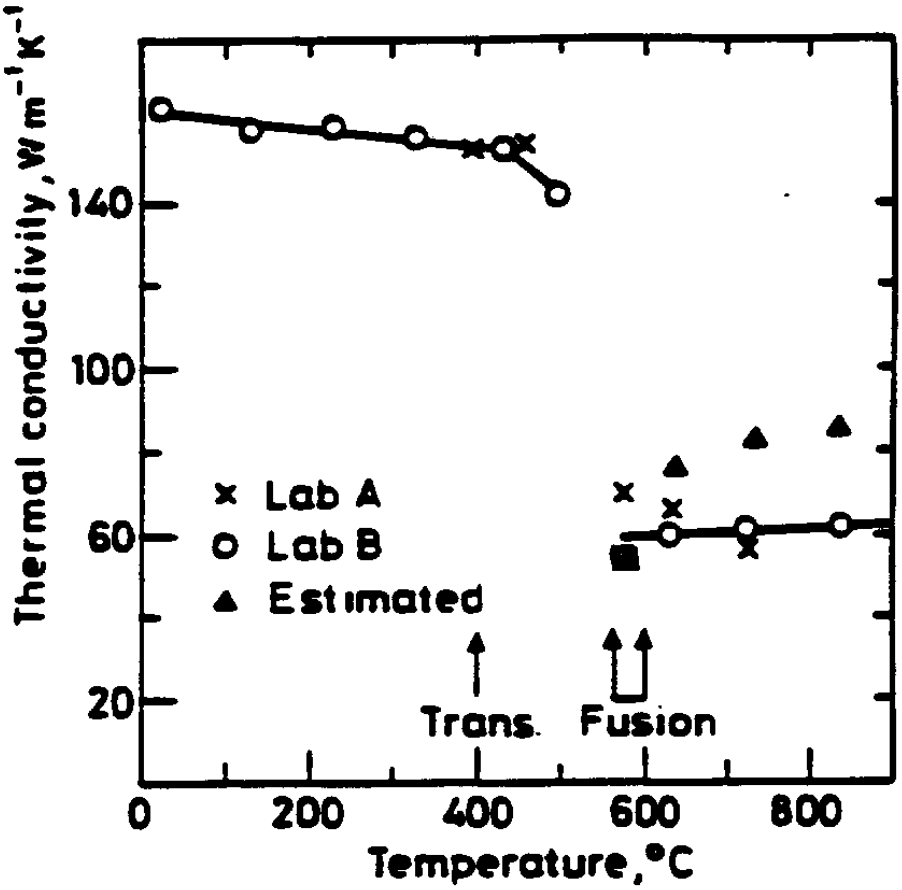


Figure 7 Thermal conductivity of an Al-Si alloy as a function of temperature; solid curve, x, o, measured values; ▲, estimated by Equations 26, 27, ■estimated by Equation 28.

## 6.2 SOLID ALLOYS

When the model based on Equations 24 to 26 was applied to the calculation of thermal conductivities of solid alloys, the calculated values were found to be much larger than those obtained experimentally. This is due to the fact that both electronic and phonon (or lattice) conduction are important at lower temperatures. Furthermore, the ratio of electronic to lattice conduction differs appreciably from metal to metal; for instance electronic conduction is the dominant mechanism for Al alloys ($\lambda^{el} >> \lambda^{lat}$) but $\lambda^{el}$ and $\lambda^{lat}$ are both important for steels and nickel-based superalloys. This means it is very difficult to develop a *universal* model and it is necessary to develop methods for particular families of alloys such as steels, superalloys, Al alloys etc.

There is also the problem that the electrical and thermal conductivities are significantly reduced by the presence of dislocations and non-metallic inclusions and these are affected by both the heat treatment and mechanical treatment of the sample. Since aluminium alloys have high thermal conductivities the latter are particularly sensitive to their thermal

and mechanical histories. The fully-annealed state has been used as the reference state and thus predicted values will tend to be higher than the values recorded for samples which have been subjected to mechanical working or heat treatments designed to precipitate second phases.

For steels, Ni-based superalloys and Ti alloys the resistance to electronic heat transfer is much higher in these alloys than in Al alloys, consequently, lattice conduction tends to be much more significant. It is therefore appropriate to consider the electronic and lattice effects separately.

$$\lambda_T = \lambda_T^{el} + \lambda_T^{lat} \qquad (29)$$

Smith and Palmer (35smi/pal) derived a relationship between thermal and electrical conductivities for various alloys. Powell (65pow) reviewed the correlation between these data for solid and liquid alloys including those based on Al, Cu, Fe, Mg, Ni, NiCr, Ti and Zr and steels.

Aluminium alloys

Powell (65pow) suggested that thermal conductivities for aluminium alloys can be fitted to an equation of the form:

$$\lambda = L\sigma T + C \qquad (30)$$

where L is of the order of 2.2E-8 $W\Omega K^{-2}$ and C about 10 $W\ m^{-1}\ K^{-1}$ and T is the temperature in kelvins. This was assumed to be valid between 0 and 300 C. It was noted that the measured values for alloys containing silicon gave larger positive differences from those predicted.

Inspection of experimental thermal diffusivity (a) data for Al alloys indicated that thermal diffusivity-temperature curves showed an increase of 5% between 298 and 573 K (25 to 300 C) and then decrease of 10% between 573 K (300 C) and the solidus temperature. This behaviour is described by Equations 31 and 32.

$$298\ K < T \leq 573\ K: \quad a_T = a_{298}\left[1+\left(\frac{T-298}{275}\right)2x10^{-2}\right] \qquad (31)$$

$$573\ K < T < T_{sol}: \quad a_T = 1.055\, a_{298}\left[1-\left(\frac{T-573}{300}\right)4x10^{-2}\right] \qquad (32)$$

where T is the temperature in kelvins.

Thermal conductivities can be calculated using the following steps:

(i) calculate $\sigma_{298}$ from chemical composition

$$\sigma_{298} = k_1(\%1) + k_2(\%2) + k_3(\%3) \qquad (33)$$

where the k values are constants derived by numerical analysis of electrical conductivity data for aluminium alloys

(ii) calculate $\lambda_{298}$ from $\sigma_{298}$ using Equation 24

(iii) calculate $a_{298}$ from $\lambda_{298}$ using the relation

$$a = (\lambda / Cp.\rho) \quad (34)$$

using estimated Cp (Equation 2) and density (Equations 10, 11) values and use Equations 31 and 32 to derive $a_T$

(iv) calculate thermal conductivities $\lambda_T$ from $a_T$ using Equation 35.

$$\lambda_T = a_T \; Cp_T \; \rho_T \quad (35)$$

Steels

Inspection of thermal conductivities - (T) curves (Figure 8) for a variety of different steels, shows that:

(a) the thermal conductivities vary by almost an order of magnitude and

(b) the temperature coefficient ($d\lambda / dT$) varies in sign according to the composition

(c) $\lambda_T$ attains a reasonably constant value around 800°C (1073 K) and then continues to rise with temperature.

Values of $\lambda_T$ as a function of temperature are calculated using the following steps:

(i) Calculate $\sigma_{298}$ using the relation, $\sigma_{298} = (\%1)k_1 + (\%2)k_2 + (\%3)k_3$, where k values were derived from numerical analysis of electrical conductivity data of annealed steels.

(ii) Calculate $\lambda^{el}_{298}$ from $\sigma_{298}$ using Equation 24.

(iii) Calculate $\lambda^{lat}_{298}$ from the chemical composition ($\lambda^{lat} = \lambda^{meas} - \lambda^{el}$) and then numerical analysis was used to determine the optimum values of c for $\lambda^{lat}_{298} = (\%1)c_1 + (\%2)c_2 + (\%3)c_3 + \ldots$

(iv) $\lambda_{298}$ for a steel of known composition can be derived from the compositional dependencies of $\lambda^{el}_{298}$ and $\lambda^{lat}_{298}$ and Equation 29.

(v) The $\lambda T$ - temperature curve is then constructed using fixed values of $\lambda_T$ of 25 and 31.5 $Wm^{-1}\,K^{-1}$ at 800°C (1073 K) and 1300°C (1573 K), respectively (Equations 33, 34).

$$298 < T \leq 1073\ K: \quad \lambda_T = \lambda_{298} + (25 - \lambda_{298})\left(\frac{T - 298}{775}\right) \tag{36}$$

$$1073 < T < 1573\ K: \quad \lambda_T = 25 + 0.013\ (T\text{-}800) \tag{37}$$

where T is the temperature in kelvins.

Nickel-based superalloys

The model used was identical to that used for steels except $\lambda_T$ at 1073 and 1573 K, respectively, were taken as 23 and 32 $Wm^{-1}K^{-1}$, respectively and different compositional constants are used.

Ti-based alloys

A similar approach was also used for these alloys except a third range was introduced to account for the or $\alpha \rightarrow \beta$ transformation which occurs between 700°C (973K) and 1000°C (1273 K):

$$298 < T \leq 973\ K: \quad \lambda_T = \lambda_{298} + (23 - \lambda_{298}\left(\frac{T - 298}{675}\right) \tag{38}$$

$$973 < T \leq 1273\ K: \quad \lambda_T = 15.2 + 0.0273\ (T - 973) \tag{39}$$

$$1273 < T \leq 1923\ K: \quad \lambda_T = 23 + 0.0075\ (T - 1273) \tag{40}$$

where T is the temperature in kelvins.

The estimated thermal conductivities are compared with measured values for various steels and for M based superalloys in Figures 8 and 9, respectively. It can be seen that the predicted thermal conductivities for solid alloys are in good agreement with the experimental values and it has been found that values are usually within ±10% of the experimental values.

This is particularly encouraging since experimental uncertainties associated with (a) the method are usually cited as ±5% and (b) the effects of thermal and mechanical treatments of the samples are probably even larger. The principal disadvantage with the model lies in the fact that the calculated values for high temperatures do not differentiate between different alloy compositions.

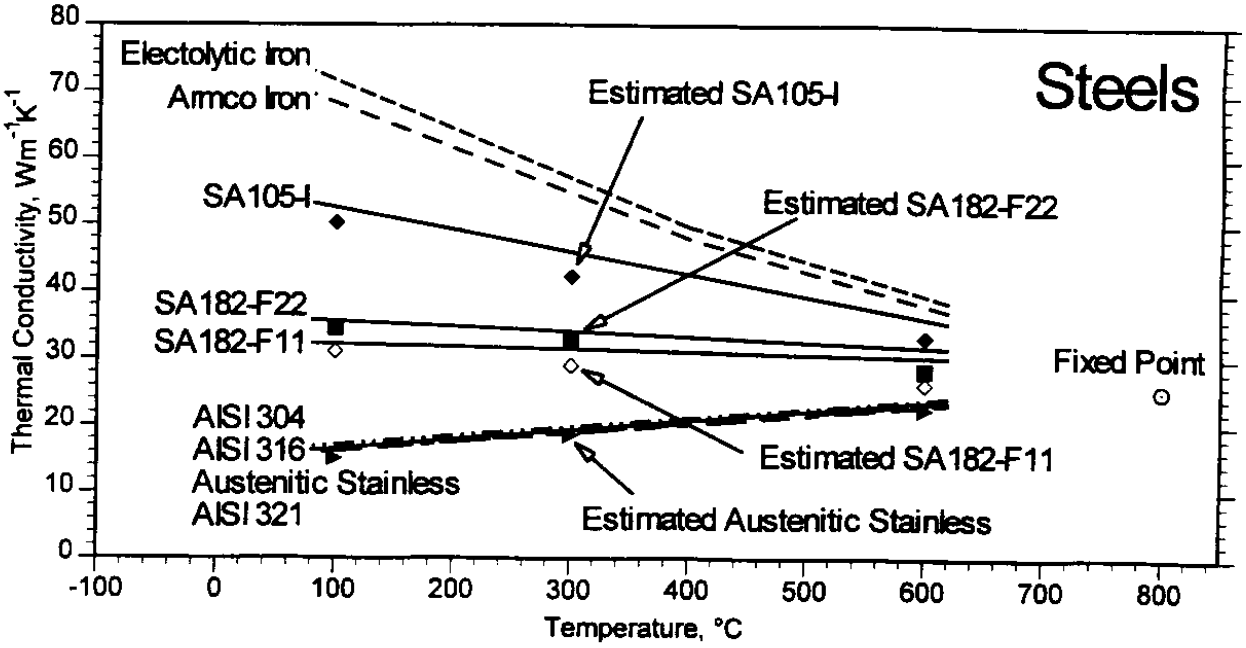


Figure 8 Thermal conductivities of steels as a function of temperature with experimental points superimposed

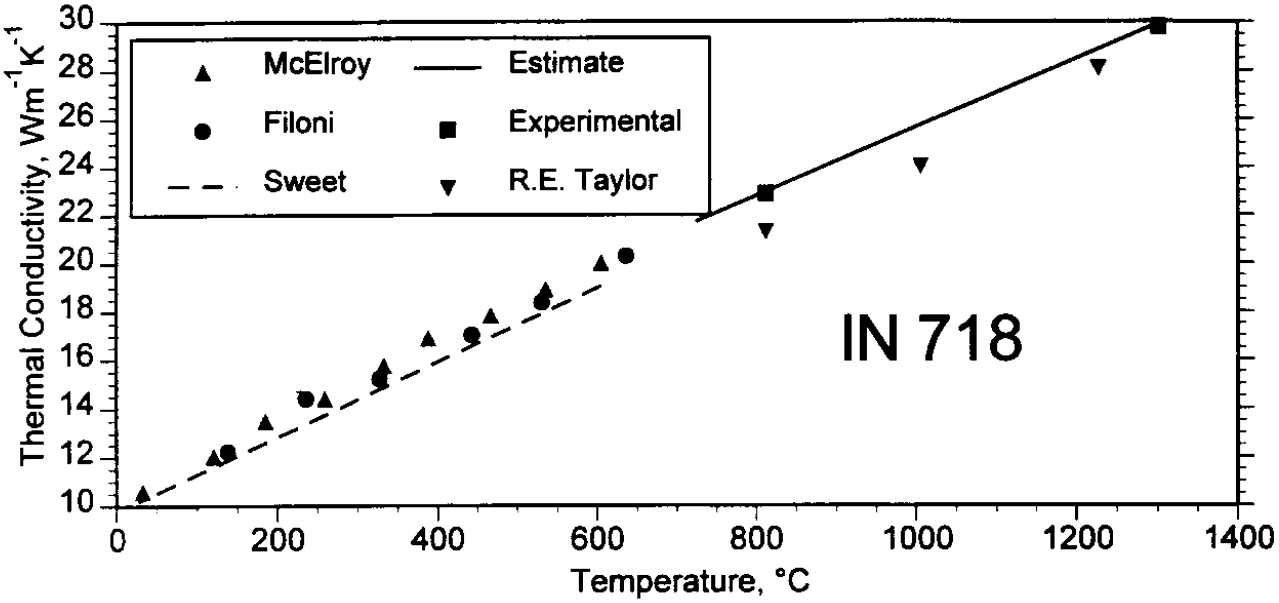


Figure 9 Thermal conductivities of Ni-based superalloy IN718 as a function of temperature with experimental points superimposed

## 6.3 ALTERNATIVE APPROACHES

For carbon and low alloy steels Miettinen [97mie] has assumed that the thermal conductivity can be expressed as:

$$\lambda = (1 + A_{mix}) f^L \lambda^L + (1 - f^L) \lambda^S \quad (41)$$

where $\lambda^L$ and $\lambda^S$ are the thermal conductivities of liquid and solid states and $A_{mix}$ is a constant value parameter describing the effect of liquid convection upon the thermal conductivity.

For both solid and liquid phases Miettinen expressed the thermal conductivity by:

$$\lambda = \lambda_{Fe} + \sum k_i C_i \qquad (42)$$

where, again, $\lambda_{Fe}$ is the thermal conductivity of pure iron, $k_i$ describes the effect of the solute i and $C_i$ is the composition of the solute in weight percent. A similar approach has been used for copper alloys [99har/mie].

A more sophisticated approach has been developed by Spittal et al (99spi/rav, 99rav/bro) who derived numerical methods for predicting an effective thermal conductivity in solid liquid regions as a function of fraction solid using a finite difference method applied to the known morphologies of the mushy zone. The authors conclude that thermal conductivity will be highly anisotropic especially if the liquid and solid thermal conductivities are very different or if the proportion of primary arm material is high in columnar dendrites.

## 7 SURFACE TENSION

Tanaka et al. [94tan/iid1, 94tan/iid2, 97tan/oga, 99tan/hac] have developed a way of predicting the surface tension $\sigma$ of binary liquid alloys and molten ionic melts using a modified Butler equation [32but] which assumes an equilibrium between the bulk liquid phase and a surface "phase" which can be thought of as the outermost monolayer:

$$\sigma = \sigma_A + \frac{RT}{A_A}\ln\frac{(1-x_B^S)}{(1-x_B^B)} + \frac{1}{A_A}\overline{G}_A^{E,S} - \frac{1}{A_A}\overline{G}_A^{E,B} = \sigma_B + \frac{RT}{A_B}\ln\frac{x_B^S}{x_B^B} + \frac{1}{A_B}\overline{G}_B^{E,S} - \frac{1}{A_B}\overline{G}_B^{E,B} \qquad (43)$$

where $\sigma_A$ is the surface tension of pure A, $A_A$ is the molar surface area in a monolayer of pure liquid A which can be obtained from:

$$A_A = L\, N_0^{1/3}\, V_A^{2/3} \qquad (44)$$

where $N_0$ is the Avogadro number, $V_A$ is the molar volume of pure liquid A and L is a constant usually set to 1.091 for liquid metals. $x_A$ is the mole fraction of component A and $\overline{G}_A^{E,S}$ and $\overline{G}_A^{E,B}$ the excess Gibbs energy in the surface and bulk "phases" respectively. The equivalent properties relating to component B are reflected in use of the suffix B eg $\sigma_B$.

Tanaka et al [94tan/iid1, 94tan/iid2, 99tan/hac] have derived equations to link the excess Gibbs energy in the surface and bulk phases. For each overall bulk liquid composition it is necessary to calculate the surface liquid composition and the total surface tension such that the above equation is satisfied. The equation can be generalised to liquids with more than two elements. Tanaka found that there was very good agreement between the predicted and experimental surface tension as shown in figure 10.

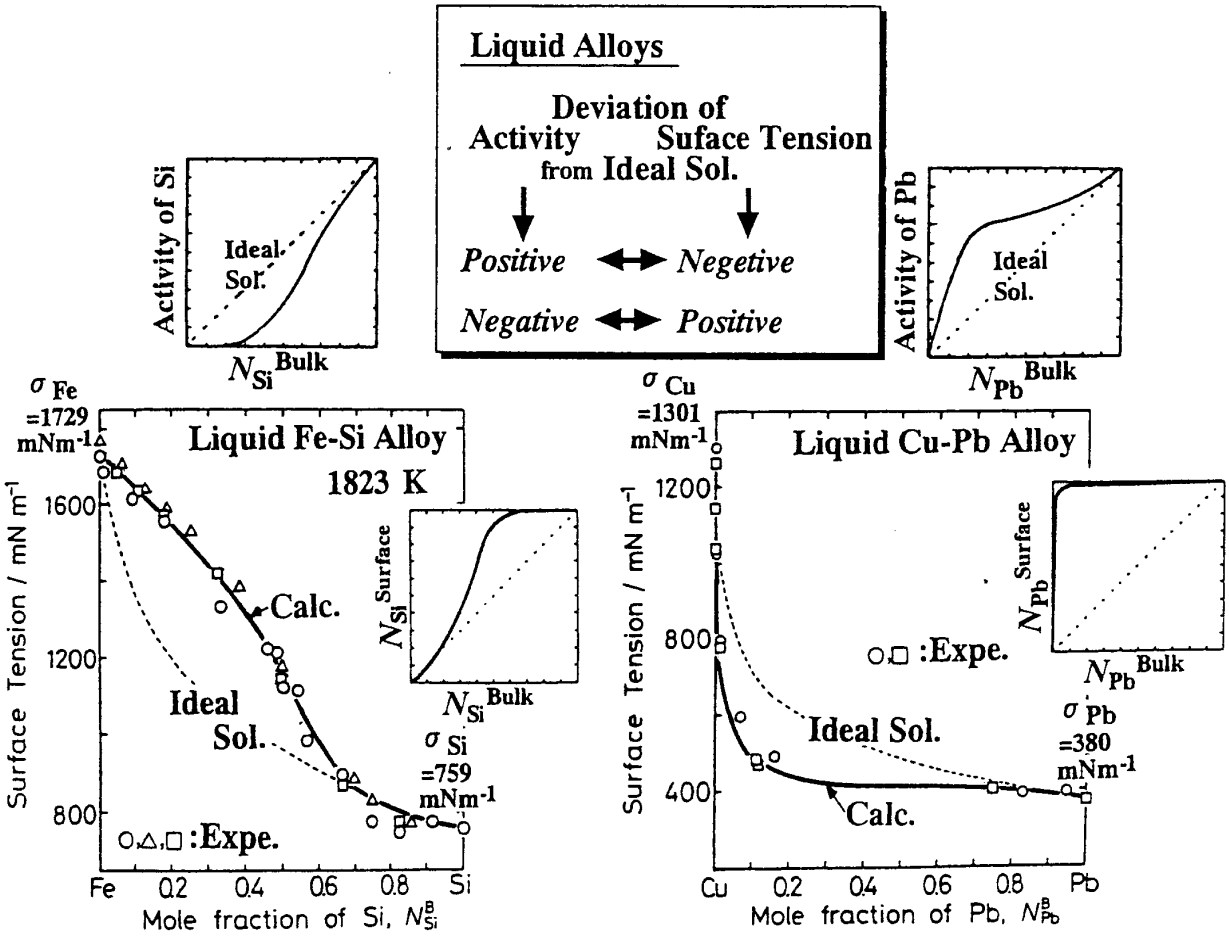


Figure 10 Example of agreement between calculated and experimental values of surface tension for Fe-Si alloys and Cu-Pb alloys.

## 8 PERMEABILITY

In the mushy zone the flow of the molten material is hindered by the existing dendrites. The ability of the liquid to flow or the permeability is generally expressed in terms of the Blake-Kozeny equation (45) [99mag]:

$$m = \frac{K(1-f_s)^3}{f_s^2} \tag{45}$$

where m is the permeability, $f_s$ is the fraction solid and K is material dependent constant.

This equation has been reformulated as the Kozeny-Carman relation [99nie/arn, 56car]:

$$m = \frac{(1-f_s)^3}{5S_s^2} \tag{46}$$

where $S_s$ is the solid-liquid interfacial area concentration ie the solid-liquid interfacial area per unit volume [99nie/arn]. The relationship between $S_s$ and dendrite arm spacing has been discussed by Wang and Beckermann (93wan/bec).

## CONCLUSIONS

1) It is possible to estimate the physical properties of multicomponent alloys from a knowledge of the chemical composition and the melting range.

2) The uncertainties in the predicted values are approximately enthalpy, heat capacity(± 2%) density (± 5%) viscosity (± 20%) thermal conductivity of liquids (< 25%) of solids (± 10%).

## ACKNOWLEDGEMENTS

The authors gratefully acknowledge the valuable contributions of Dr Jack Counsell and Helen Quested.

## REFERENCES


32but Butler, J A V, Proc. Roy. Soc. London, Ser. A 135 (1932) 348

34and Andrade, E N daC: Phil.Mag. 17 (1934) 497-732

34mot Mott, N F: Proc. Royal Soc. A146 (1934) 465.

35smi / pal Smith, C S, Palmer, E W, Trans. Amer. Inst. Min. Metall. Engrs., 117 (1935) 225-243

41gla / lai Glasstone, S, Laidler, K J, Eyring H: *The theory of rate process*, McGraw-Hill Book Co., NewYork, NY (1941)

60pow Powell, R W, The Engineer (1960) 929-732

65pow Powell R W, Int. J. Heat Mass Transfer 8 (1965) 1033-1045

70tou / pow Touloukian, Y S, Powell, E W, Ho, C Y, Klemens, P G: Thermophysical Properties of Matter, Vol 1, Thermal conductivity of metallic elements and alloys, publ. IFI / Plenum, New York, (1970).

71lud / sch Ludwigson, D C, Schwerer, F C: Metall Trans. 2 (1971) 3500-3801

74stu Stubbs, G B: *The Nimonic Alloys and other nickel-based high temperature alloys* ed. W Betteridge and J Heslop, Chapter 10. (1974) 157-185

75mor / spo Morrow, III H, Sponseller D L, Semchyshen M, Metall. Trans. A 6A (1975) 477-485

80tur Turkdogan, E T: *Physical Chemistry of High Temperature Technology*, Academic Press, New York (1980).

87fil / roc Filoni, L, Rocchini, G: High Temp-High Pressure 19 (1987) 381-387

88bog / ho Bogaard, R H, Ho C Y: Thermal conductivity 19 (1988) 551

88kaw / shi Kawai Y, Shiraishi, Y: *Handbook of Physico-chemical Properties at High Temperatures*. Special Issue No 41, publ IS1J, Tokyo (1988).

89fil / roc Filoni, L, Rocchini, G: High Temp-High Pressure 21 (1989) 373-376

89iid / gut Iida, T, Guthrie, R L: *The Physical Properties of Liquid Metals* (Clarendon, Oxford) 1989.

91din Dinsdale, A T: CALPHAD, 15 (4) (1991), 317-425.

93bog / des Bogaard, R H, Desai P D, Li H H, Ho, C Y: Thermochimica Acta 218 (1993) 373 393.

93hir Hirai, M: Iron Steel Inst. Jpn. Int., 33(2) (1993) 251-8

93kub / alc Kubaschewski, O, Alcock, C B, Spencer, P J. *Metallurgical Thermochemistry*, Pergamon, London. 1993

93wan / bec Wang C Y, Beckermann C, Metall. Trans. A, 24A (1993) 2787-2802

94mie / lou Miettinen, J, Louhenkilpi, S: Metall. Mater. Trans. B 25B (1994) 909-916

94see / du Seetharaman,S, Du Sichen: Metall. Metall. Mater. Trans. B; 25B (1994) 589-595

94tan / iid1 Tanaka, T, IidaT: Proc. Conf. International Symoposium on Science and Technology of Metallurgical Processing - The Morita Symposium ed T. Emi and M. Iguchi (1994) 7-12

94tan / iid2 Tanaka, T, Iida T: Steel Research 65 (1994), 21-28

95que Quested, P N: Unpublished physical property data, National Physical Laboratory, (1995).

95que / mil Quested, P N, Mills, K C, Brooks, R F: Proc. Conf. Modelling of Casting, Welding and Advanced Solidification Processes to be held in London, Sept 1995, pub. TMS.

96mil / kee Mills, K C, Keene, B J, Monaghan, B: Int. Mater. Rev. 41(6) (1996) 209-242 "Thermal conductivities of molten metals"

97mie Miettinen, J: Metall. Mater. Trans. B 28B (1997) 281-297

97sun / poi Sung, P K, Poirier, D R, McBride, E, Mater. Sci. Eng. A231 (1997) 189-197

97tan / oga Tanaka, T, Ogawa, M, Ueda. T, Hara S: Proc. Conf. Molten Slags, Fluxes and Salts, (1997) 263-267

98sun / poi Sung, P K, Poirier, D R, Mater. Sci. Eng. A245 (1998) 135-141

99har / mie Härkki, K, Miettinen, J: Metall. Mater. Trans. B 30B (1999) 75-98

99mag MAGMASOFT reference book, 1999

99rav / bro Ravindran K, Brown S G R, Spittle J A, Mater. Sci. Eng. A, A269 (1999) 90-97

99spi / rav Spittle J A, Ravindran K, Brown S G R, Modelling Simul. Mater. Sci. Eng. 7 (1999) 59-70

99tan / hac Tanaka, T, Hack, K, Hara, S: MRS Bulletin, (1999), 45-50

# APPENDIX

## Experimental and numerical methods for determining the solidification path in commercial alloys.

J D. Hunt,
Dept. of Materials,
University of Oxford.

Most metallic alloys solidify from the melt at some stages in their processing. If equilibrium occurred, at the end of the process each phase would have a uniform composition and the quantities of the phases would be determined by the phase diagram using the lever rule [1]. This would mean that the alloy became solid at the equilibrium solidus temperature.

In practice equilibrium freezing cannot occur in any continuously cooled process. Large departures occur particularly as the last liquid freezes. The quantities and distribution of the phases and even the phases that are present may be different from that expected from equilibrium considerations.

Information about the non-equilibrium process is needed for a number of reasons. It may be necessary to modify microstructure to obtain particular properties, to input enthalpy evolution as a function of temperature in a casting model, to provide fraction solid as a function of temperature or to control the freezing range. The latter may be important in models of macrosegregation, hot tearing or recrystallisation.

General solidification terminology and the physical process of microsegregation are described in the first sections. It is the microsegregation that determines the non-equilibrium fraction solid and the freezing range. Other sections consider experimental methods for measuring microsegregation, fraction solid as a function of temperature, and the non-equilibrium freezing range. The later sections consider the numerical models that have been used to calculate microsegregation. The limitations of the models and the difficulties that arise because of lack of physical property data are then discussed.

### A1. The problem:

When an alloy solidifies solid nucleates and grows into a grain. Under some conditions columnar grains are formed while in others new grains are continuously formed producing an equiaxed structure [eg. 2]. Each grain will generally consist of many cells or dendrites. It is usually suggested that dendrites have secondary arms but cells do not. Segregation over the scale of cell / dendrite spacing is microsegregation. Segregation over distances large compared with the cell / dendrite spacing is called macrosegregation.

If a material is grown directionally, planar growth occurs at the lowest growth rate, as the growth rate is increased first cells and then dendrites are formed. As the growth rate is further increased, high velocity cells are formed and eventually the front becomes planar again [3]. In many commercial casting processes alloys freeeze with a dendritic or high velocity cellular front. When dendrites or cells grow the concentration of solute is different at the centre and towards the edge of the single phase cell / dendrite and this is defined as microsegregation.

## A1.1 Microsegregation.

Microsegregation arises because solid is deposited over a range of temperatures. For the alloy $C_0$ shown in figure A1, the first solid to be deposited near the dendrite tip might be given by $C_{S1}$. As the solid is deposited solute is rejected into the gap between the dendrites. The local composition at the solid-liquid interface follows the phase diagram. In this case, solid deposited at a high temperature is purer than that deposited at a low temperature. Although the liquid between the dendrites can be assumed to be almost homogenous, significant composition differences will build up in the solid phase so producing microsegregation.

## A1.2 Maximum microsegrgation.

One of the simplest approximations for calculating the amount of microsegregation is to assume that the liquid is completely mixed and that the solid composition does not change once it has been deposited. This approach gives the maximum possible microsegregation. In this model, it is assumed that all the rejected solute is pushed sideways into the gap between the solid and so increases the liquid composition. This means for a binary system

$$(C_S - C_L)dg_L = g_L dC_L \qquad \text{(A1)}$$

where $g_L$ is the fraction liquid, $C_S$ is the solid composition and $C_L$ is the liquid composition. Replacing $C_S$ by $kC_L$ where $k$ is the distribution coefficient (defined as $k=C_S/C_L$) and integrating assuming $k$ is constant gives the Scheil equation

$$C_L = C_O g_L^{k-1} \qquad (\text{or} \quad C_S = kC_O g_L^{k-1}) \qquad \text{(A2)}$$

The fraction liquid can be written as

$$g_L = \left(\frac{C_O}{C_L}\right)^{1/(1-k)} = \left(\frac{T_O}{T}\right)^{1/(1-k)} \qquad \text{(A3)}$$

where $T$ is temperature. The latter form assumes the liquidus line is straight, has a slope of $m$ and the zero temperature is taken to be the melting point of the pure material; then $T_O = mC_O$ and $T = mC_L$. Equation (A3) can be plotted to give fraction solid as a function of temperature and this is shown by the filled line in figure 2. The temperature can be related to distance by assuming the temperature gradient in the semi-solid is approximately constant. This means the figure is a very distorted cell / dendrite shape.

The fraction liquid assuming equilibrium freezing can be obtained from the lever rule

$$g_{LE} = \frac{C_O - C_S}{C_L - C_S} = \frac{C_O - kC_L}{C_L - kC_L} = \frac{T_O - kT}{T(1-k)} \qquad \text{(A4)}$$

The equilibrium fraction solid is shown by the dotted line in figure A2. A point to notice is that $g_L$ is very different from $g_{LE}$ near the equilibrium solidus where $g_L$ remains finite but $g_{LE}$. = 0. The difference arises because the solid has a uniform composition which

changes with temperature in equation (A4). From equations (A3) and (A4) it is apparent that $g_L \rightarrow g_{LE}$ when $k \rightarrow 0$.

The Scheil equation and the lever rule are two extremes. In practice the microsegregation will be less than that given by the Scheil equation because of three main effects:

- The cell/dendrite tip does not grow at the equilibrium liquidus temperature.
- Diffusion occurs within the solid phase.
- Melting and re-freezing of previously solidified material takes place.

The three effects are discussed below.

### A1.3 The cell/dendrite tip growth temperature.

Near a directionally grown cell or dendrite tip the liquid between the cell/dendites cannot be considered to be homogenous as was assumed in the derivation of equation (3). Instead, solute is rapidly rejected by the tip. The build up of solute decreases the tip growth temperature and increases the solute deposited in the solid and thus decreases the amount of microsegregation.

In the extreme case of growth with a planar front, as steady state is reached the solid is deposited with the same concentration as the bulk liquid. Under this condition there is no microsegration and the growth occurs at the solidus temperature.

When a dendrite grows into a low temperature gradient, solute is rejected from the dendrite tip. The solute layer extends about one tip radius from the tip. Under this condition, the dendrite primary spacing is much larger than the tip radius so the diffusion fields at the tip do not overlap appreciably. This means very little solute is pushed ahead of the front, instead most solute is pushed into the gap between the dendrites thus causing microsegregation.

When cells grow in a high temperature gradient, the growth temperature approaches that for a planar front. The tip temperature and interface shape are plotted schematically for dendrites, cells and the planar front in figure A3, assuming no diffusion in the solid . The plots are shown with that predicted by the Scheil equation from figure A2. If no diffusion occurs in the solid, the distance from the right hand axis is proportional to the solid composition. Thus it can be seen that there is considerable microsegregation for dendrites, much less for cells and none for a planar front.

Accurate cell/dendrite growth temperature may be calculated using analytical expressions [4] obtained by fitting numerical results. In summary growth far from the alloy liquidus temperature decreases the amount of microsegregation.

### A1.4 Diffusion within the solid phase.

As discussed earlier, if no diffusion occurred in the solid the final segregation would be a result of the amounts of solid deposited at the different temperatures. This was the extreme case approximated by the Scheil equation. In practice even though the diffusion coefficients in solids are typically three to four orders of magnitude smaller than those for liquids, appreciable diffusion occurs in the solid because large times are involved. A

calculated plot of solid and liquid compositions at different temperatures is shown in figure A4. Each line represents the composition at a given time/temperature. The solid composition is less than that in the liquid. The point to notice is that the composition of the centre of the cell/dendrite gradually increases as solid is deposited as a result of solid state diffusion. This diffusion will reduce the amount of microsegregation. The treatment of the solid state diffusion is usually the most important part of a theoretical treatment of microsegregation. Typically fast diffusing elements approach the lever rule whereas slow diffusing elements show significant microsegregation.

### A1.5 Melting and freezing during solidification.

During dendritic growth some of the solid deposited at a high temperature is remelted. The remelting occurs during the secondary arm coarsening process and because of temperature gradient zone melting TGZM [5].

When dendrites grow the initial secondary arm spacing is much finer than that at lower temperatures. During growth some of the arms continue growing while others melt back [6]. The process is surface energy driven and has much in common with Ostwald ripening [7]. When columnar dendrites form the secondary arms move up the dendrite stem. This is the result of a concentration gradient between the dendrites resulting from the change in temperature. The flux of solute in the liquid can lead to melting on one side of a secondary arm and more rapid growth on the other [8]. This process is similar to TGZM [5].

Melting of solid deposited at a high temperature and replacing it with additional material deposited at a lower temperature reduces the amount of microsegregation.

### A1.6 Microsegregation in multi-component alloys.

The discussion so far has considered two components; similar considerations apply in commercial alloys where many components are present. When more than two components are present the tip growth temperature and composition will be influenced by the liquid diffusion coefficient for each component. At lower temperatures diffusion within the solid will be very different for different elements. As an example calculations indicate that in aluminium alloys Fe approaches a Scheil distribution whereas Si becomes almost homogenised [9]. It is usually assumed that the flux of an element depends only on the concentration of that element. In fact the flux will depend, often to a lesser extent, on the concentration gradients of all the other elements. Neglect of this effect will probably be important when both interstitial and substitutional elements are present.

At first sight it might be concluded that the difference between the two extremes of microsegregation as shown in figure A2 are not very different. The major difference appears as the liquid fraction becomes small. It is often very difficult to accurately predict when the last liquid freezes. This might be important in trying to predict when a casting begins to gain strength. If only one solid phase is involved freezing the last liquid is a result of diffusion in the solid state. This means that non-equilibrium solidus is often very much lower than the equilibrium solidus. One implication of this is that eutectic or peritectic phases may appear even though they should not be present from equilibrium considerations.

In multicomonent alloys the path over the liquidus surface depends on the extent of the microsegregation. It is probable that the quantity of eutectic will be larger than expected from equilibrium considerations. When peritectic like reactions are involved the quantity of the higher melting point phase will be larger than expected. In some cases the initial single phase growth will be limited by reactions involving other phases which are local equilibrium phases but not equilibrium phases.

## A2 Experimental measurement of microsegregation and fraction solid as a function of temperature.

Various methods have been used to measure microsegregation. Measuring the non-equilibrium quantity of eutectic using optical techniques is a simple direct method. Electron optical techniques such as the electron microprobe or EDX may be used to measure composition. Line traces on transverse sections of directional grown sample can be used to investigate the composition change from the centre of a cell or dendrite; similarly line traces on lengthwise sections have shown saw-toothed composition profiles on secondary arms that are expected when TGZM occurs [10]. Difficulties arise in ensuring measured results are typical when only one section is investigated. A widely used technique which gives more representative results is that proposed by Gungor [11]. A grid is set up with a mesh size larger than the typical microstructure and the composition is measured at mesh corners. The composition is measured at a point which has an effective size small compared with the microstructure. A composition interval is chosen and the number of measurements within the range are counted and divided by the total number of points to give the area fraction (and thus volume fraction) for that composition interval. The composition can then be plotted against fraction by summing the volume elements.

It is difficult to measure fraction liquid as a function of temperature. Even with transparent materials it is difficult to allow for the liquid surrounding irregular dendrites, similar problems arise when Xray methods are used [12]. An alternative, widely used technique is to quench a directionally grown sample. Examples are shown in figure A5 [13]. The figure shows transverse section of three directionally grown peritectic alloys. Knowing the temperature gradient and temperature at one point allows the temperature of each section to be calculated. The left hand micrographs show primary dendrites surrounded by liquid. The peritectic phase has started growing in the second from left. A decreasing amount of liquid and an increasing amount of the peritectic phase occurs as the temperature decreases. In this type of experiment there will always be uncertainty as to whether the quench is rapid enough to show the growth interface. Good results are only possible when the cooling rate during the quench is about $10^4$ to $10^6$ faster than that during directional growth (estimated by noting the secondary arm spacing is approximately proportional to the freezing time raised to the power of a third [14]).

Other indirect methods such as scanning calorimetry can also be used to give an estimate of the fraction solid as a function of temperature. In the simplest approach the enthalpy versus temperature plot is extrapolated below the liquidus temperature and the enthalpy when completely solid is extrapolated to higher temperatures where melting has started (see figure A6). During cooling, the fractional distance between the lines gives a measure of the latent heat still to be evolved. Knowing the enthalpy change for each of the phases allows the fraction remaining liquid to be estimated. Figure A6b shows the estimated fraction solid measured using a single-pan DSC [15]. Problems arise in practice since it

may not be possible to extrapolate the enthalpy of solid from a low temperature because heat is evolved for reasons other than melting. Other serious problems arise in a conventional two-pan heat flux calorimeter if the raw data is not corrected for temperature smearing [15].

Potentially any physical property that is different in the solid and liquid phase might be used to estimate fraction solid. One such is the average electrical conductivity which has been used to estimate average thermal conductivity [16]. The electrical conductivity could in principal be used to give the fraction liquid provided the conductivity of each phase was known as a function of temperature and an allowance could be made for the changing composition in the liquid and possible composition gradients within the solid. Similar problems might be expected to arise with techniques which measure the speed of sound [17].

In summary techniques are available to measure the results of microsegregation optically and electron optical techniques are available to measure concentration profiles after solidification. The physical property which varies most significantly between liquids and solids is enthalpy. For this reason it is suggested that improved scanning calorimetric techniques are the most promising for investigating the fraction solid as a function of temperature.

## A3. Theoretical models of microsegregation.

A large number of microsegregation models have been proposed over the last thirty years. In their review Kraft and Yang [18] mention 63 and others could be added to the list. The initial models carried out Scheil type calculations eg [19]; later models attempted to allow for tip undercooling effects [20]. Other workers attempted to allow for diffusion in the solid anlalytically [21,22], these models were crude and did not allow the variation in diffusion coefficient with temperature. Kirkwood [23,24] and co-workers [25,26] considered back diffusion in the solid using numerical methods and established the importance of considering the variation in diffusion coefficient with temperature. Attempts have been made to allow for coarsening and TGZM effects [27,28].

None of the treatments can be considered to be a complete description of the solidification process. All simplify the solidification problem so that analysis can be made. The aim in this section will be to describe, as an example, the model "Alloy" [9] written by the author and to examine the approximations which have been made in this and other microsegregation models. The two component version of the program "Alloy" treats solidification in some fifty binary system. Phase diagram information and other data are stored in a data base. The numerical model handles primary phase, eutectic and peritectic growth. First the alloy composition and growth conditions are selected and the program is run. During a run, the cooling curve, microsegregation plot and a schematic microstructure is displayed. About eighty copies of the binary program have been distributed (copies are available with the instruction manual on request). The multicomponent version is being developed; the program calls MTDATA for phase diagram information at each cycle and at present can treat single phase solidification.

Both the binary and multicomponent versions use the same diffusion solver. This can handle any number of components and any number of phases. At present it is assumed

that the flux of a component depends only on the composition gradient of that component (this restriction could be removed relatively easily).

The basic assumption made in the model is that a thin section such as that shown in figure A7 is analysed as the alloy freezes. The section starts at the tip of the dendrite and is then cooled to room temperature. It is assumed that there is no appreciable loss of solute from the section in the dendrite growth direction. This assumption was examined with a three dimensional cell/dendrite model [4] and found to be valid except near the dendrite tip. In "Alloy" allowance is made for diffusion in the tip region by assuming that the initial fraction liquid is given by the fraction that would be present at the cell/dendrite growth temperature at equilibrium. The assumption is unlikely to be very wrong once the diffusion fields near the dendrite tip have overlapped; that is about one primary spacing behind the tip. This assumption deals with the effect discussed in section A1.3 and is similar to that made by other workers.

As a slice cools, the composition in contact with the boundary between the phases is forced to follow the phase diagram. The change in composition at the boundary leads to diffusion and the movement of the boundary. If solid and liquid are present as the slice cools solidification occurs. If solid state diffusion is negligibly small, the variation in solid composition reproduces the Scheil equation and if the solid diffusion coefficient is large almost complete mixing occurs in both the solid and liquid. Any intermediate amount of diffusion is automatically treated by the program.

When a peritectic reaction occurs a new solid phase is introduced between the solid and liquid. The growth of the new phase is determined by the interface conditions and diffusion in the three phases a b and liquid. When a eutectic is formed a new pseudo single phase is considered to have been produced. The phase is assumed to be single phase because only one length scale is treated in the present model. If the eutectic was being fully treated, diffusion and the effect of curvature would be necessary on the scale of the eutectic. In the model the pseudo single phase is deposited with the same composition as the liquid.

An implicit control volume technique is used [29]. Each phase is divided up into a number of control volumes (or boxes). A careful account is then made of the fluxes of solute into a box to give the change in composition inside the box. The flux through a control volume wall is the diffusive flux and that due to the motion of the wall. The accumulation of solute within a control volume takes into account the fluxes and the change in volume. The numerical technique is implicit; that is the composition and position at all the control volume centres at the end of the time step are used to calculate fluxes which would change the starting composition to the final composition. The fluxes are calculated by either using an upwind approximation or central difference approximation [29].

The boundary between phases is placed at a control volume centre. The control volumes within a phase expand or contract as a phase grows or shrinks. An accumulation of solute equation exists for each control volume. As mentioned earlier, the calculated compositions must also be consistent at each phase boundary with the phase diagram at the relevant temperature. This boundary condition between the phases provides an additional equation that allows the boundary motion to be calculated. Since the model is implicit any time step is mathematically stable and the only limitation on step is loss of physical

accuracy. A Newton Raphson technique is used to solve the non-linear simultaneous equations. Usually three iterations are needed to give errors limited by double precision accuracy (typically $10^{-12}$ in composition). All control volumes within a phase have the same size. The control volume size will generally be different for each phase. The size is monitored at each time step and changed by altering the number of control volumes within that phase; when the size is greater than 1.45 times the average size, more boxes are created; when the size is less than 0.69 the average size, boxes are removed. The new compositions and position of the box centres are obtained by interpolation. The minimum number of boxes is taken to be two. The time step is adjusted during a run so that no wall moves more than two box spacings.

Controls within the program allow the central difference or upwind approximation to be used and allow planar or axi-symmetry to be imposed. Three different growth modes (cooling or heating modes) can be imposed:
1) In the first steady state directional growth is assumed. This would apply when a specimen is pulled from a furnace or during the directional growth of a turbine blade. The temperature drop in a time interval is that necessary to account for latent heat evolution and any change in conductivity resulting from the change in fraction of the phases.
2) The second mode simply assumes the cooling rate is constant. Since the cooling rate can be changed at will during the run, this means that a cooling curve, for example from a DC casting, can be exactly reproduced.
3) The third mode assumes a constant rate of heat extraction. In this mode the temperature at the end of the time step is calculated by the model. This mode produces cooling curves similar to those obtained during traditional thermal analysis or during differential thermal analysis.

Clearly a dendrite cannot really be described by planar or axi-symmetry. A complete treatment of a three dimensional dendrite is not possible. The trick used in the "Alloy" program and in all approximate descriptions of microsegregation is based on the assumption that reasonable results can be obtained if a suitable length scale and the correct solid state diffusion coefficient is used. The difficulty comes in deciding how to choose the length scale as a function of alloy composition and growth conditions. The numerical models mentioned earlier can be used to predict cell and dendrite primary spacing as a function of the growth conditions. Analytic expressions have been obtained by fitting the numerical results [4]. For the cellular structure it is reasonable that the diffusion length scale should be the primary cell spacing. For dendrites a suitable length scale is more difficult to justify. In the present work, fractions of the primary spacing are arbitrarily assumed to be valid. The fraction is chosen by considering the relative contribution due to gradient term and the velocity term. The fraction is gradually changed from 0.5 to 0.25 [9]. These values are based on experience and are at least qualitatively correct. Another approach is to use a spacing given by coarsening kinetics [25] or alternatively using previously measured values. What is used as the diffusion distance is the weak step in all numerical models of this type.

In "Alloy" no direct allowance is made for coarsening or TGZM, it is suggested that an increased solid state diffusion coefficient would produce a similar effect. The problem is that the coarsening or TGZM cannot be treated with any rigour. The difficulty is that it is not possible to estimate the fraction of each solid composition that is melted nor is it possible to estimate the quantity of material that is melted. All that really happens, when an oversimplified model is used is that additional adjustable parameters are introduced.

Despite these reservations reasonably accurate predictions can be made. Quenched interface sections in three peritectic systems were shown in figure A5 to illustrate quenching as an experimental technique. These and other sections were used to measure the quantity of each of the phases as a function temperature. A comparison of the measurement with prediction is shown in figure A8a, b and c. The points are the experiment and the lines the prediction. Very good agreement has been obtained but it should be realised that the solid state diffusion coefficients have been fitted since none were available. The values estimated do not appear to be unreasonable. It is of interest to note that the initial fraction solid calculated by the model for dendritic growth is reasonable justifying the treatment of the dendrite tip.

## A4. The value of the approximate models

What must be admitted is that none of the models is completely rigorous. The question then is how valuable are they? Their main value must be in the increase of understanding. The use of the Scheil equation to describe microsegregation instead of assuming equilibrium cooling was a step forward; but unfortunately it led too easily to the assumption that the Scheil distribution always occurs. The use of diffusion models by Kirkwood and others showed the importance of back diffusion. It quickly became apparent that only a small change in the solid state diffusion coefficient changes conditions from approaching the Scheil limit and to that approaching the lever rule. It also became apparent that the temperature dependence of the diffusion coefficient plays an important role in understanding microstructure. The models allow widely held assumptions to be tested. As an example it is usually stated in textbooks that cooling something slowly will eliminate microsegragation. Using the models it can easily be shown not to be true. When a material is slowly cooled the structure is coarser so that back diffusion is more difficult and this compensates for the additional available time. Although the models are not rigorous they are quantitative so the assumptions and improvements can be tested. An essential feature for future use of models is the availability of solid state diffusion data.

## A5. Other theoretical approaches.

A great deal of interest has recently arisen on phase field modeling [30-33]. This is a very powerful technique that allows the interface between the solid and liquid to be modelled in detail. It is possible to produce two-dimensional dendrites growing from a nucleus reproducing the dendrite tip and arms. Microsegregation occurs as does the coarsening process. Single dendrites are begining to be produced in three dimensions. The problem with this approach is that it is extremely computer intensive. Considerable computing time is needed on the fastest computers available to allow one dendrite to grow for a short time. It is clear, however, that eventually many dendrites and dendrite arrays will be treated first in binary systems then in multi-component systems. When this occurs it will possible to model the solidification path over the multi-component liquidus surface with considerable rigour. Accuracy will be possible if the phase diagram and diffusion data are available; in addition it will be necessary to have data on solid-liquid surface energies and even on the anisotropy of the surface energy. In this authors view there are formidable obstacles to be overcome become the approach can expect to be used as a predictive tool for treating microsegregation.

## A6 Conclusions

Understanding and modelling microsegregation is an industrially important problem. At present, the simplified back diffusion models provide the most realistic method for getting quantitative results. It is probable that within the next decade more detailed modelling such as the phase field method will allow more rigorous analyses to be made. In future as now the numerical work will be limited by the lack of data and in particular the lack of diffusion data.

**References:**


1. RE Reed-Hill and R Abbaschian, "Physical Metallurgical Principles 3rd Edition", PWS Publishing Company, 1994, p 327.
2. SC Flood and JD Hunt, in Metals Handbook, Ninth Edition Volume 15 Casting, ASM Publishing 1988, p130-136.
3. WW Mullins and RF Sekerka, J. Applied Physics, **35** (1964) 444.
4. JD Hunt and S-Z Lu, Metallurgical and Materials Transactions A, **27A** (1996) 611.
5. WG Pfann, "Zone Melting", John Wiley, New York, 1958, p. 254.
6. KA Jackson, JD Hunt DR Uhlmann and TP Seward, Trans. Met. Soc AIME, **236** (1966) 149.
7. JW Martin and RD Doherty, "Stability of Microstructures in Metallic Systems", Cambridge University Press, 1976, p173-209.
8. DJ Allen and JD Hunt. Met.Trans., **7A** (1976) 767.
9. JD Hunt and RW Thomas, SP97 Proceedings of the 4th Decennial Conference on Solidification Processing, Sheffield University 1997, p 350.
10. DJ Allen and JD Hunt. Solidification and Casting of Metals, Proceeding of the Sheffield Conference 1977, published by the Metals Soc 1979, p39-43.
11. MN Gungor, Metallurgical Transactions A, **20A** (1989) 2529-2533.
12. PD Lee and JD Hunt, Scripta Materialia, **36 No 4**, (1997) 399-404.
13. HP Ha and JD Hunt, Metallurgical and Materials Trans A, to be published Feb 2000
14. MC Flemings, "Solidification Processing", McGraw Hill 1974, p150.
15. HB Dong and JD Hunt, accepted for publication in the Proceedings of the 15th European Conference on Thermophysical properties Sept 1999
16. B Monaghan, private communication 1999
17. C Scurby, communicated to AWD Hills 1999.
18. T Kraft and YA Chang, JOM , Dec 1997 p 20.
19. R Mehrabian and MC Flemings, Metallurgical Trans, **1** (1970) 455.
20. RM Sharp and MC Flemings, Metallurgical Trans, **4** (1973) 997.
21. HD Brody and MC Flemings, Trans. Met. Soc. AIME, **236** (1966) 615.
22. TW Clyne and W Kurz, Met. Trans, **12A** (1981) 965.
23. AJW Ogilvy and DH Kirkwood, Appl Sci Res, **44** (1987) 43.
24. AA Howe and DH Kirkwood, Solidification Processing, 1987, Institute of Metals London 1988, p 63
25. AA Howe, Appl Sci Res, **44** (1987) 51.
26. AA Howe, Modeling of casting, welding and advanced solidification processes V, (TMS 1991) p 461.
27. A Mortensen, Met. Trans, 19A (1989) 247.
28. AWD Hills and JT Duncombe, Modeling of casting, welding and advanced solidification processes VII, (TMS 1995) p 467.

29. SV Patankar, "Numerical heat transfer and fluid flow", Hemisphere Publishing USA, 1980, p30-31.
30. R Kobayashi, Physica D, **63** (1993) 410
31. AA Wheeler, WJ Boettinger and GB McFaddon, Phys. Rev A, **45** (1992) 7424.
32. G. Caginalp and W Xie, Phys Rev E, **48**, (1993) 1897.
33. JA Warren and WJ Boettinger, SP97 Proceedings of the 4th Decennial Conference on Solidification Processing, Sheffield University 1997, p 422.

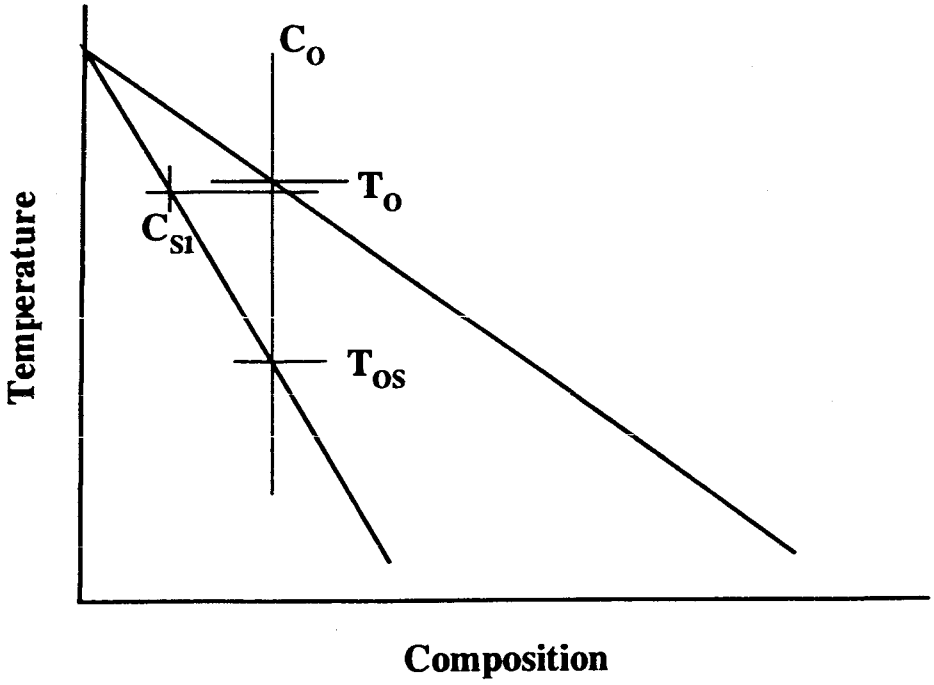


Fig A1 Schematic phase diagram showing liquidus $T_o$, solidus $T_{os}$ for composition $C_o$.

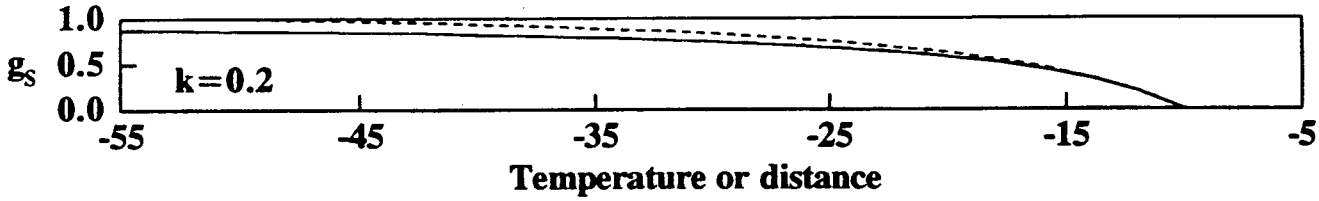


Fig A2 Plot of fraction solid as a function of temperature/distance assuming the Scheil equation (filled line) and the lever rule (dotted line).

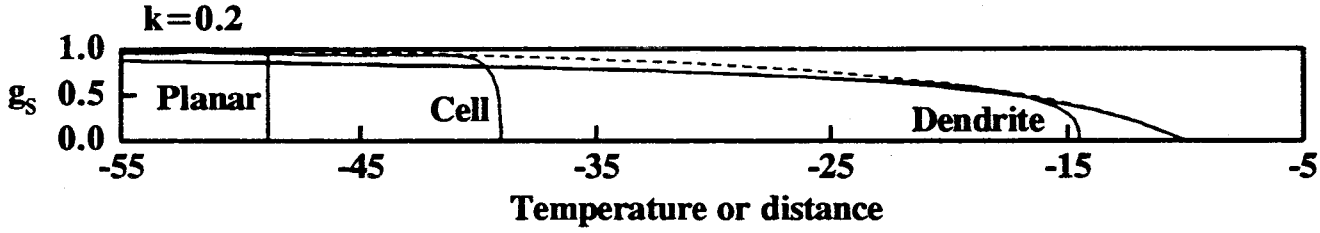


Fig A3 Plot of fraction solid as a function of temperature/distance assuming no diffusion in the solid for the Scheil equation, a dendrite, a cell and a planar front.

System: BiPb

Input data:

Pb 9.98 at% Bi: Cooling mode: Steady state growth

Tip velocity = 65.9 μ/s  Temperature gradient = 9.46K/mm

Cooling rate at tip = 0.62 K/s

Calculated data: First solid Lead rounded dendrites

Primary spacing = 130.7 μ  Diffusion distance = 65.3 μ

Tip undercooling = 2.55 K

Microsegregation

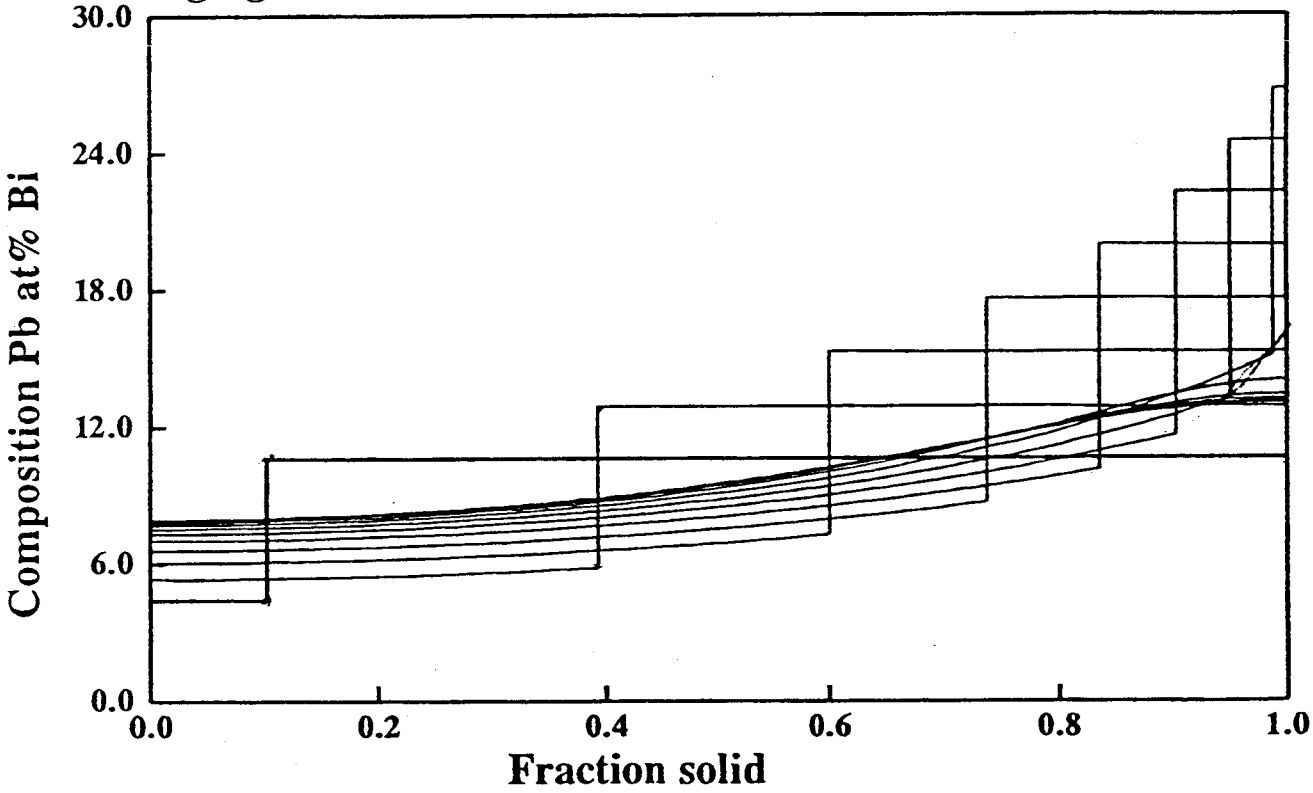


**Fig A4 Example run of composition in the solid and liquid in the BiPb system. Plots have been made every 9K.**

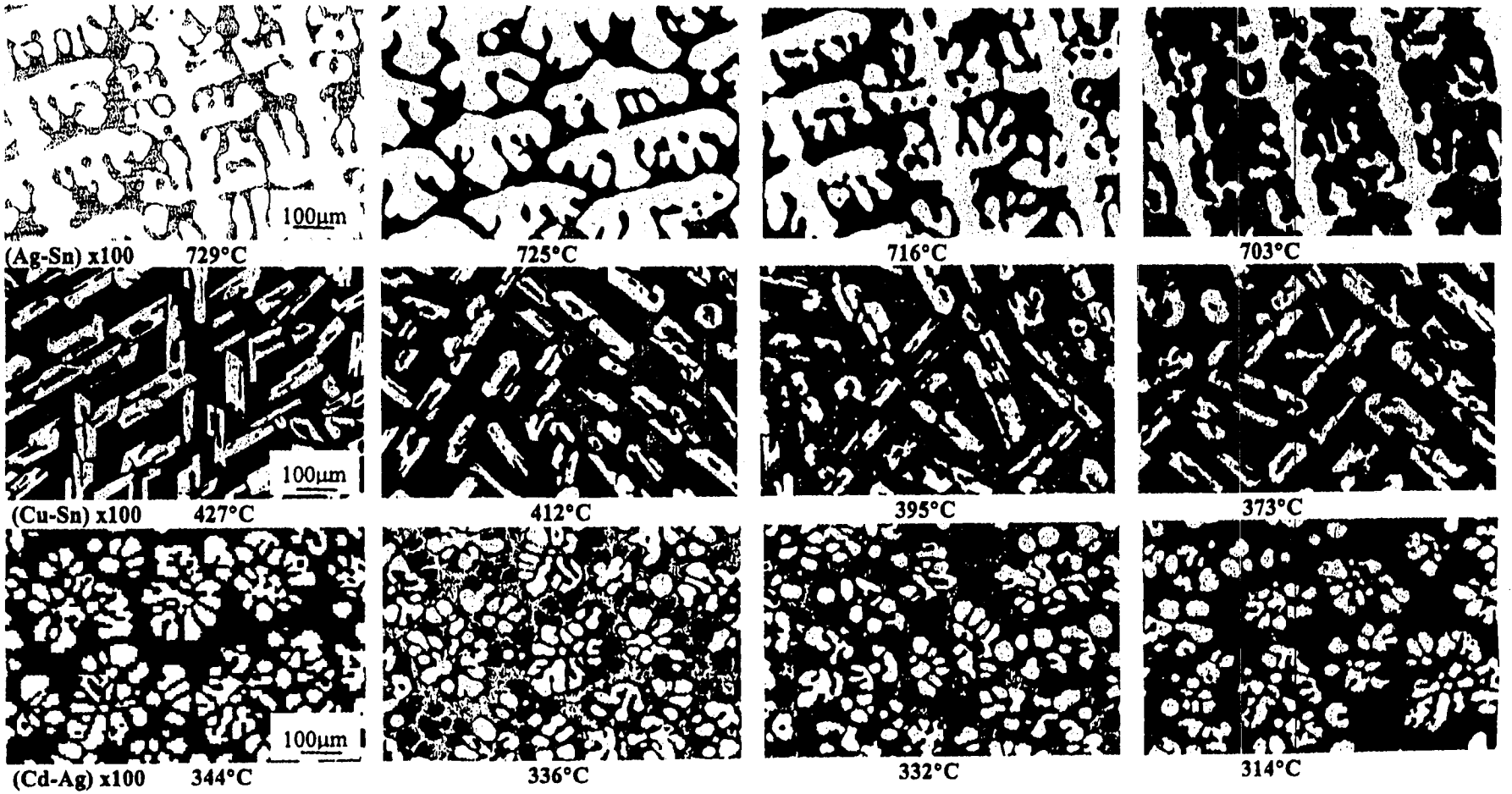


**Fig A5 Cross sections showing the variation of the volume fractions of the peritectic products as a function of temperature in Ag-14wt%Sn, Cu-78wt%Sn and Cd-8wt%Ag alloys.**

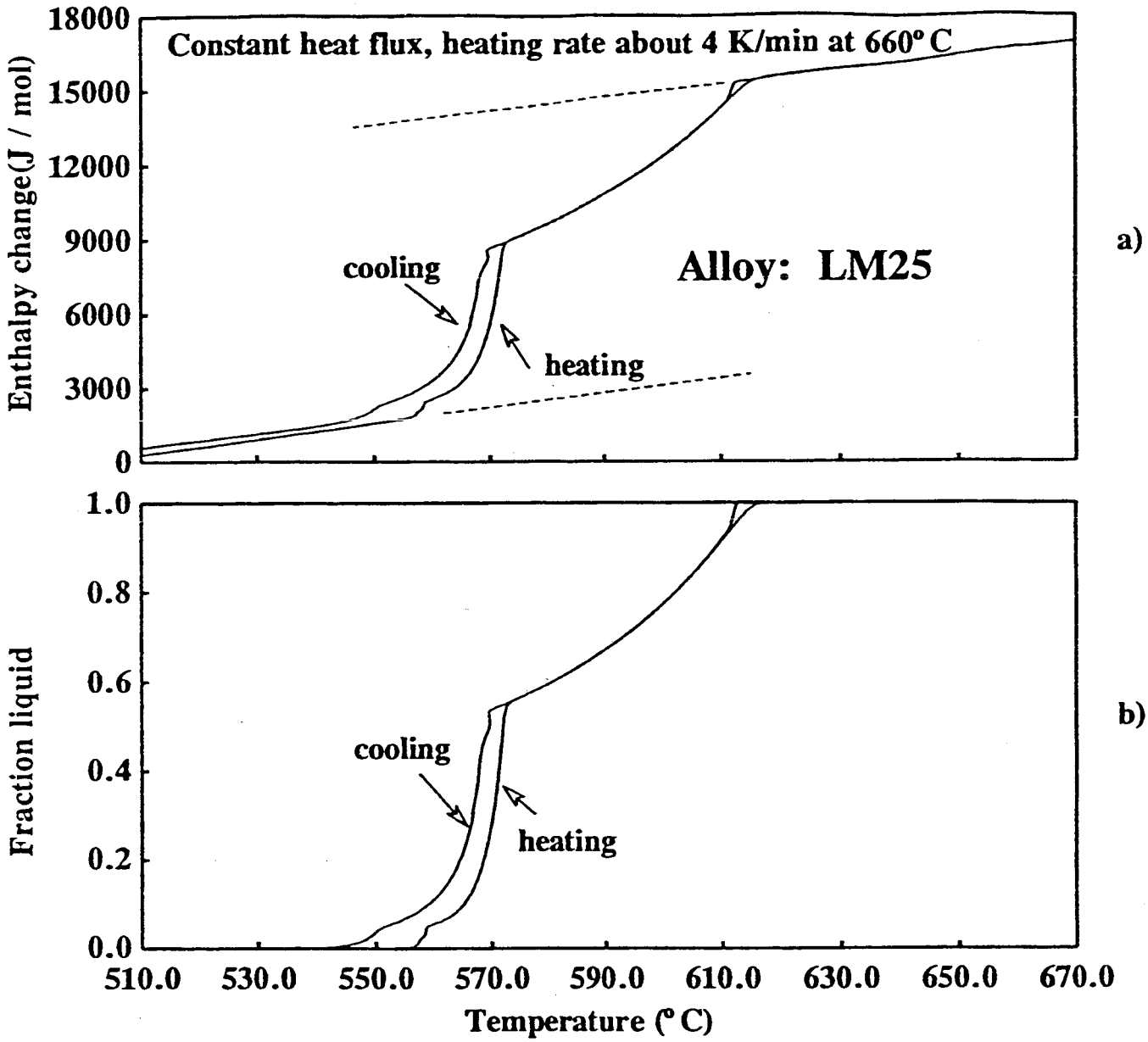


**Fig A6 Results for LM25 measured using a single-pan DSC [15] a) Measured enthalpies. b) Estimated fraction solid.**

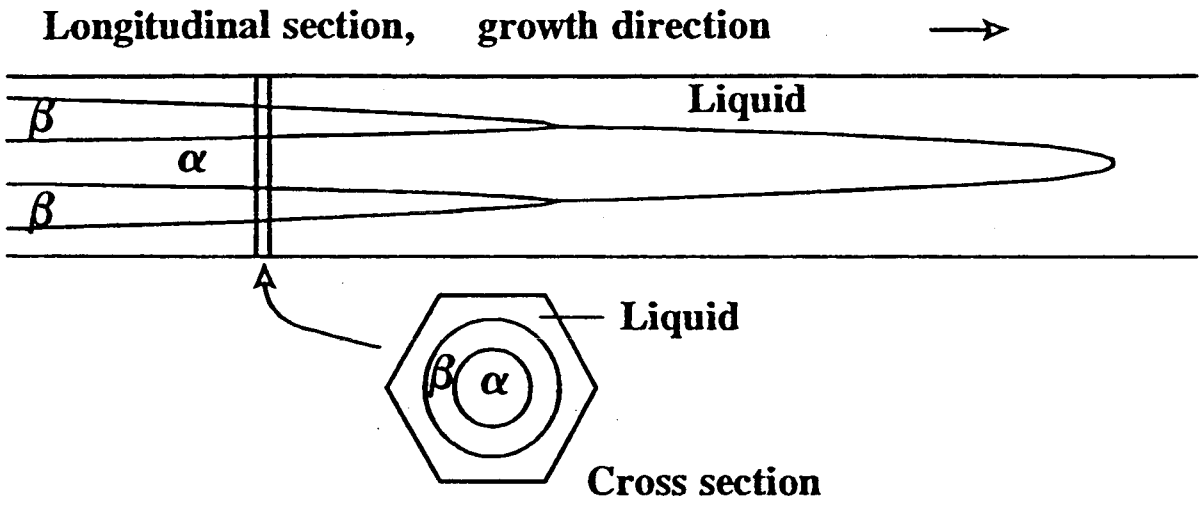


**Fig A7 Schematic diagram showing section treated in the numerical model.**

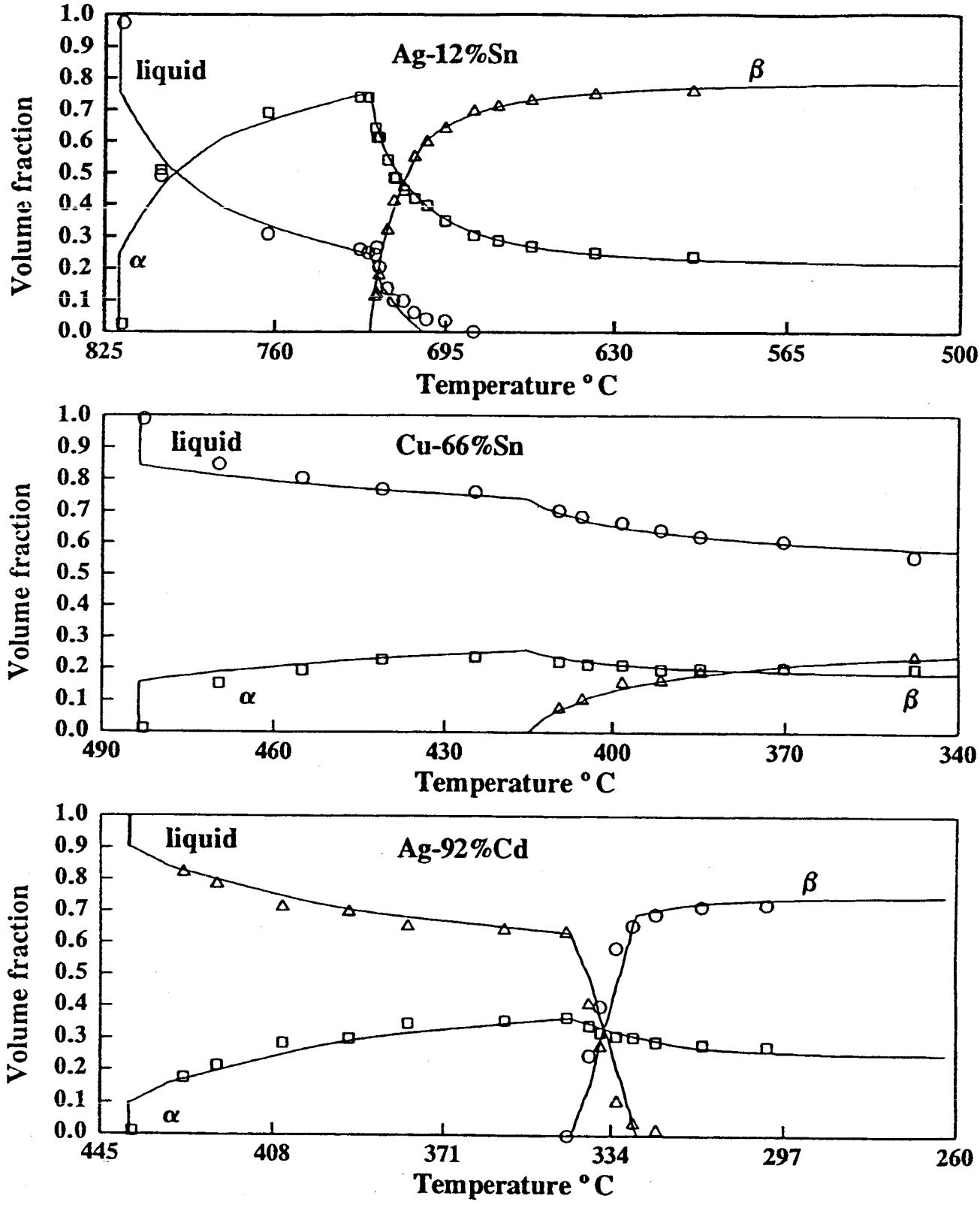


**Fig A8 Experimental fraction of the phases shown in figure 5 (points) to be compared with those calculated using "Alloy" [4] (lines).**